

We thank the reviewer for their comments, which we have discussed in the responses below and which we believe have significantly improved the manuscript.

**1.1 Regarding the methods, I am afraid that the authors have overlooked a significant part of the recent scientific literature on the subject. The voxel-based approach which is presented, tested and discussed in the manuscript is not an undisputed reference method and has a number of known drawbacks.**

We agree with the reviewer's view that a "best approach" to voxel-based PAI estimation remains contested. However, the aim of this paper is not to evaluate all possible voxel methods, but rather use a method with broad applicability to multiple TLS configurations. We chose the voxel-based method used in this study for clear reasons. First, we wanted to use full plots and segmented trees, so methods developed with single scans were inappropriate. Further, many radiative transfer methods require information on scanner location and beam direction limiting use to single scans or individual trees with known scan locations around them – not available in many TLS datasets. In addition, our preference where possible is to use methods that have been thoroughly and independently validated – in this case the voxel method chosen has been validated with destructive sampling. Finally, we only use methods that were open source and easily reproducible, excluding many insufficiently documented, GUI-based or proprietary approaches. Further discussion of our choice is given in our answer to the following comment.

We note that efforts to move towards a best practice consensus are building within the community requiring a dedicated effort and we believe our study provides direction for ways forward. We also highlight that methods should be compared across sensor and forest types to draw robust conclusions. As the data used in this study are published, we would be delighted to see further exploration of this topic making use of different voxelisation schemes but see the testing of these different methods to be beyond the scope of this study.

**1.2 L103-106 the authors briefly mention that there are different approaches to voxel-based estimation of PAI/LAI and they opt for one that treats elementary voxels as either empty or full (opaque). Unfortunately, there is no obvious justification for such a choice being made. The emerging consensus in the recent literature seems to be in favour of what the authors refer to as "simulating radiative transfer within each cube". One significant advantage being that the laser scanning geometry is considered, and hence the variable sampling intensity and occlusion effects on PAI estimated can be accounted for.**

While we appreciate the reviewer's comment that significant recent progress has been made in the field, our view is that a consensus on best approach is yet to be reached and the approach proposed by the reviewer is still contested (and please see the proceeding comment). In particular, there is increasing recognition that voxel size significantly influences PAI/WAI/LAI estimates, and many methods do not provide clear guidance on how to deal with this. For example, You et al., (2022), published after the submission of this manuscript, argue that voxel-based methods are highly sensitive to voxel size and present a morphology-based method to obtain LAI from the surface area on envelope fitting to extracted leaf points. A key benefit of the voxel-based approach used in this study is the clear justification for matching voxel size to point cloud resolution, as evaluated in Li et al., (2016) and validated using destructive samples. Using a radiative transfer approach PAI estimates are highly unstable over varying voxel sizes and there is no clear guidance from the literature on how to choose the correct one. Evaluating the many potential methods for calculating LAI from TLS data are well beyond the scope of this study, however, we hope that the work presented here will contribute towards a future consensus in the field.

As discussed in our response to reviewer 2 (comment 2.9), we have amended our discussion of voxel size in section 1.3 to reflect the debate around voxel size choice, L108-113:

*"However, PAI estimates derived using the voxel method are highly dependent on voxel size (Calders et al., 2020). Using a radiative transfer approach, Béland et al., (2014) demonstrated that voxel size is conditional on canopy clumping, radiative transfer model assumptions and occlusion effects, making a single, fixed choice of voxel size within methods for all datasets impossible. To test various approaches to selecting voxel size using a voxel classification approach, Li et al., (2016) matched voxel size to point cloud resolution, individual tree leaf size, and minimum beam distance and tested against destructive samples, finding that voxel size matched to point cloud resolution had the closest PAI values to destructive samples."*

To clarify our justification for use of a voxel classification approach over a radiative transfer approach, also commented on by reviewer 1, we have added to section 2.4 (L199-201):

*"We chose a voxel classification approach as this method is widely applicable to a range of TLS systems and levels of processing as well as providing explicit guidance on voxel size selection, which is known to impact derived PAI estimates (Li et al., 2016)."*

**1.3 In addition, degrading point cloud resolution down to the voxels resolution is likely to degrade the quality of point cloud segmentation into leaf and wood as well as the PAI estimates.**

Downsampling is a critical step in *treeSeg* (Burt et al., 2019) to handle computational loads associated with segmenting point clouds. We thank the reviewer for drawing attention to our lack of clarity over the justification for down sampling data and have added to L220-224:

*"We used individual tree point clouds downsampled to 0.05 m, to aid computation time, and segmented using the automated tree segmentation program treeSeg (Burt et al., 2019), implemented in C++, by Owen et al., (2021) for that study. Individual segmented tree data are available in Owen et al., (2022)."*

The requirement of individual tree point clouds in *TLSeparation* means downsampled individual tree point clouds are necessary without upscaling the resolution of individually segmented trees. The scale of this study (2472 trees, 33 plots) means using a raw data resolution is computationally impracticable and consequently, downsampling is common practice in studies using large datasets of individual tree point clouds. We believe choosing a *knn* based on the point cloud resolution is a robust approach to optimising wood leaf separation under the constraints associated with large datasets. We explain the *knn* in L229-231 of the submitted manuscript:

*"The knn of each iteration is directly dependent on point cloud density, since high density point clouds will require higher a knn (Vicari et al., 2019). We used the utility package in TLSeparation to automatically detect the optimum knn for each tree point cloud."*

We chose point cloud resolution as a trade-off between computational demands while retaining the structural information contained in each tree. We then matched voxel size to point cloud resolution rather than down sampling point cloud resolution to desired voxel size. This is in line with recommendations for the method we chose; many voxel-based methods provide no clear guidance on this. We thank the reviewer for drawing attention to our lack of clarity here and have added to L195-199:

*To calculate PAI using the Voxel-Based method, we followed a voxel classification approach (Hosoi and Omasa, 2006), downsampling the point cloud to 0.05 m to aid computation time and matching the voxel size to the resolution of the point cloud, following Li et al., (2016), who showed that matching the voxel size to the point cloud point to point minimum distance (resolution) increases accuracy as small canopy gaps are not included in voxels classified as vegetation.*

**1.4 For these reasons, I believe the conclusions drawn are not well grounded. The general conclusion that “Our results demonstrate the challenges that stand in the way of large scale adoption of TLS for vegetation indices monitoring” which refers to the large discrepancies observed between methods in their study contradicts recent papers such as (Béland and Kobayashi, 2021; Nguyen et al., 2022). Obviously, there are still challenges to address but this study does not seem to identify the real caveats associated with the use of TLS in vegetation studies.**

From the cited literature we assume the reviewer is referring to (1) voxel size and (2) occlusion.

Regarding voxel size, we agree that there is a major problem in choosing voxel size with little consensus on how to choose the correct one for a range of forest types and ecosystems (see responses above). Separate analysis performed within our group shows unstable results over a range of voxel sizes using a radiative transfer approach, with a wide range of derived indices for one scan across relatively small variation in voxel size, suggesting high model sensitivity to this input parameter. The method we chose matches the voxel size to the resolution of the point cloud, and while the reviewer has pointed out there are “a number of known drawbacks” with this method, we feel that in the absence of well justified methods this is a pragmatic approach to accurately choosing the correct voxel size, and has been validated with destructively sampled data.

Regarding occlusion, Béland and Kobayashi, (2021) have chosen a very dense scanning density (5 m between scans), which is impractical in large-scale forest plots, and greater than the suggested scanning density in Wilkes et al., (2017), making such a dataset rarely available. Béland and Kobayashi, (2021) also suggest site specificity for their results, focusing on broadleaf trees, limiting the applicability of findings to our mixed Mediterranean forest.

Finally, the conclusion reached in our paper that “challenges stand in the way of large scale adoption of TLS” are drawn from a comparison of three TLS methods with conventional DHP. Neither papers cited (Béland and Kobayashi, 2021; Nguyen et al., 2022) test a voxel-based method against other widely used TLS PAI derivation methods (e.g. LiDAR pulse, 2D intensity image) and DHP, rather they are focused entirely on a voxel-based approach. We therefore argue the novelty of our findings and believe they do not contradict these papers.

**1.5 Both theory and algorithms have advanced significantly in recent years and convergent approaches to PAI/LAI estimates from lidar (both TLS and ALS) are emerging. Maybe the authors will want to check the following references**

We thank the reviewer for the references provided, however, argue that our dataset is significantly different from the data used in these studies. Methods suggested by the reviewer have been developed with individually scanned trees or branches (e.g. Béland et al., 2011; Soma et al., 2018), or with simulated data (e.g. Grau et al., 2017; Pimont et al., 2019, 2018; Soma et al., 2020). Individually scanned trees or branches can be scanned with a set of known scan positions allowing the precise location, distance, and beam angle from the scanner to be derived. Further, Béland and Kobayashi, (2021) focused on broadleaf

trees functionally and physiologically different to those in our study, used a prohibitively dense scanning strategy (5 m), and lack validation from destructive sampling. Our dataset comprises 2472 trees scanned from 528 locations. To derive point-level information containing scanner location and beam angle would add significant complexity and computational load to the study. While an important question, understanding the necessity for this added complexity is beyond the scope of this paper.

As stated in the proposed manuscript L26-28: *"Our findings highlight the value of TLS data to improve fundamental understanding of tree form and function, but also the importance of rigorous testing of TLS data processing methods at a time when new approaches are being rapidly developed."*, we argue that the purpose of this paper is not to evaluate the latest methods, rather to take a step back and test existing methodologies with a large dataset.

**1.6 the authors refer to Beland et al. 2014 when noting the potential role of voxel size in the voxel-based approach, but that paper uses a voxel-based approach which is not the one used by the authors**

Thank you for pointing out this inappropriate reference to Béland et al., (2014); we apologise for this mistake and have corrected it in L346, changing the reference to Li et al., (2016) who found voxel size to have significant effect on PAI estimates using the same voxel-based approach used in the study.

**1.7 Regarding the ecological insights, the clearest result seems to be that the alpha parameter (WAI/PAI) decreases with tree size (figure 6). The interpretation of what may appear as a paradox is largely speculative. It is interpreted as the result of competition but no data supporting this is presented. One might have tried to explore how alpha evolved in relation to the local competition index for instance.**

We thank the reviewer for the suggestion of exploring how alpha evolves with local competition, which is a key finding of this paper that we have not sufficiently highlighted. Figure 6b shows how alpha changes in relation to plot-level crown area index (CAI), a measure of the plot area covered by tree crown, and one that we have used as an indicative measure of local competition.

To clarify the use of CAI as indicative measure of local competition, we have changed the wording in L246-249 to state:

*"To further understand observed drivers of variance in PAI, we tested the relationship between PAI and TLS estimated whole plot crown area index, CAI, calculated as the sum of projected crown area divided by the plot area (Owen et al., 2021), and a proxy measure of stand density and local competition (Caspersen et al., 2011; Coomes et al., 2012), using SMA."*

**1.8 There is abundant literature (and theoretical arguments) that indicate that LeafToWood biomass ratio of trees growing in stands will tend to decrease with size (Bartelink, 1997; Forrester et al., 2017; Mensah et al., 2016). In the present study, the WoodToLeaf area ratio is found to decrease with tree size (for the four species for which there is a significant trend in figure 6). This could be an artefact as the authors point out (l. 387-394). The issue might indeed have to do with the leaf/wood filtering.**

We agree with the reviewer that there is abundant literature that argue leaf to wood biomass ratio will tend to decrease with size, however, the literature cited by the reviewer differ fundamentally from our study in ways that may explain differences in results. For example, the focus species, *Fagus sylvatica* in Bartelink, (1997) is functionally different to species

analysed in this study; Forrester et al., (2017) evaluate leaf biomass rather than wood to plant ratio and Mensah et al., (2016) omit correction for competition in their models while also excluding the largest trees from the study possibly introducing bias. This means that the arguments presented may not hold in our dataset measured in a mixed Mediterranean forest.

We agree that wood to plant ratio could be influenced by an artifact of wood – leaf classification, and have elaborated on this point in L418-425 of the proposed manuscript: *“Wood may be harder to accurately classify than leaves in TLS data (Vicari et al., 2019), resulting in a higher occurrence of false positives in wood clouds, potentially leading to an overestimation in WAI, and therefore underestimation of  $\alpha$ , especially in trees with small leaves which are prevalent in dry, Mediterranean environments (Peppe et al., 2011). The problem of misclassification will increase in taller trees due to TLS beam divergence, occlusion and larger beam footprint at further distances (Vicari et al., 2019), suggesting that WAI overestimation could be more pronounced in tall trees. Although our dense scanning strategy (Owen et al., 2021) was designed to mitigate some of these effects, it is possible our findings could underestimate the slope of the negative relationship between  $\alpha$  and tree height.”*. Based on this, we would expect to be underestimating the negative slope of the relationship between alpha and tree height if it was an issue of misclassification.

**1.9 This is also a field where progress has been made in recent years and maybe the authors would want to test alternative algorithms to TLSeparation which might perform better on their data. Some pointers are given below**

We agree that there has been progress in the field of wood – leaf classification, however, we argue most progress has been focused on scaling wood – leaf classification from individual trees to whole scan or plot data (e.g. Krisanski et al., 2021; Wan et al., 2021; Wang, 2020; Wang et al., 2018; Wu et al., 2020) rather than major improvements in the classification framework itself. In the case of LeWoS (Wang et al., 2020), the tool has been tested only with tropical trees and, although, distributed as open-source, is either in the form of Matlab code or a pre-compiled executable, substantially limiting wider applicability. Testing the multitude of available approaches to wood – leaf classification would be invaluable to the field, however, is beyond the scope of this study – not least because such a test should use destructively sampled validation data, which we do not have access to. Here we are interested in using well-established methodology that has been validated with a range of tree types, so based our choice on that criteria.

**1.10 My overall appreciation is that the data collected is very significant and could indeed contribute some new insights in terms of tree/forest ecology but more work is needed prior to publication.**

We thank the reviewer for their comments and appreciate that the reviewer recognises the significance of our data and results. We are confident that following their and the other reviewer's comments that the manuscript has been significantly enhanced.

**1.11 Reprocessing the TLS data already segmented using an open source freely available code incorporating much of the latest theoretical improvements should not take long. This analysis may profoundly alter the reported results (i.e the large overestimation of PAI with a voxel-based approach and the unexpected negative trend in WAI/PAI with increasing tree size). This may help clarify whether leaf/wood segmentation may be an issue and require further scrutiny or not.**

Whilst additional analyses are always possible, in this case we believe our methodological choices are defensible, and these have been discussed in previous responses. We use well-

established and tested leaf separation and PAI estimation methods that were tested, in the case of voxel-based method, with destructive samples. The scope of this study is to benchmark the most rigorously available methods, not testing all available methods but taking the conservative approach. Further, all the methods tested in this study are either open source in common programming languages, or, where we have written code this has been made freely available. Not all the methods suggested by the reviewer are open source or easily integrated into automated workflows. We believe that running the analysis again would introduce new, different biases, and don't believe this would enhance manuscript without changing scope.

## References

- Bartelink, H.: Allometric relationships for biomass and leaf area of beech (*Fagus sylvatica* L), *Ann. For. Sci.*, 54, 39–50, <https://doi.org/10.1051/forest:19970104>, 1997.
- Béland, M. and Kobayashi, H.: Mapping forest leaf area density from multiview terrestrial lidar, *Methods in Ecology and Evolution*, 12, 619–633, <https://doi.org/10.1111/2041-210X.13550>, 2021.
- Béland, M., Widłowski, J.-L., Fournier, R. A., Côté, J.-F., and Verstraete, M. M.: Estimating leaf area distribution in savanna trees from terrestrial LiDAR measurements, *Agricultural and Forest Meteorology*, 151, 1252–1266, <https://doi.org/10.1016/j.agrformet.2011.05.004>, 2011.
- Béland, M., Baldocchi, D. D., Widłowski, J.-L., Fournier, R. A., and Verstraete, M. M.: On seeing the wood from the leaves and the role of voxel size in determining leaf area distribution of forests with terrestrial LiDAR, *Agr. Forest Meteorol.*, 184, 82–97, <https://doi.org/10.1016/j.agrformet.2013.09.005>, 2014.
- Burt, A., Disney, M., and Calders, K.: Extracting individual trees from lidar point clouds using treeseg, *Methods Ecol. Evol.*, 10, 438–445, <https://doi.org/10.1111/2041-210X.13121>, 2019.
- Caspersen, J. P., Vanderwel, M. C., Cole, W. G., and Purves, D. W.: How Stand Productivity Results from Size- and Competition-Dependent Growth and Mortality, *PLoS ONE*, 6, e28660, <https://doi.org/10.1371/journal.pone.0028660>, 2011.
- Coomes, D. A., Holdaway, R. J., Kobe, R. K., Lines, E. R., and Allen, R. B.: A general integrative framework for modelling woody biomass production and carbon sequestration rates in forests, *Journal of Ecology*, 100, 42–64, <https://doi.org/10.1111/j.1365-2745.2011.01920.x>, 2012.
- Forrester, D. I., Tachauer, I. H. H., Annighoefer, P., Barbeito, I., Pretzsch, H., Ruiz-Peinado, R., Stark, H., Vacchiano, G., Zlatanov, T., Chakraborty, T., Saha, S., and Sileshi, G. W.: Generalized biomass and leaf area allometric equations for European tree species incorporating stand structure, tree age and climate, *Forest Ecology and Management*, 396, 160–175, <https://doi.org/10.1016/j.foreco.2017.04.011>, 2017.
- Grau, E., Durrieu, S., Fournier, R., Gastellu-Etchegorry, J.-P., and Yin, T.: Estimation of 3D vegetation density with Terrestrial Laser Scanning data using voxels. A sensitivity analysis of influencing parameters, *Remote Sensing of Environment*, 191, 373–388, <https://doi.org/10.1016/j.rse.2017.01.032>, 2017.
- Hosoi, F. and Omasa, K.: Voxel-Based 3-D Modeling of Individual Trees for Estimating Leaf Area Density Using High-Resolution Portable Scanning Lidar, *IEEE T. Geosci. Remote*, 44, 3610–3618, <https://doi.org/10.1109/TGRS.2006.881743>, 2006.

Krisanski, S., Taskhiri, M. S., Gonzalez Aracil, S., Herries, D., and Turner, P.: Sensor Agnostic Semantic Segmentation of Structurally Diverse and Complex Forest Point Clouds Using Deep Learning, *Remote Sensing*, 13, 1413, <https://doi.org/10.3390/rs13081413>, 2021.

Li, Y., Guo, Q., Tao, S., Zheng, G., Zhao, K., Xue, B., and Su, Y.: Derivation, Validation, and Sensitivity Analysis of Terrestrial Laser Scanning-Based Leaf Area Index, *Can. J. Remote Sens.*, 42, 719–729, <https://doi.org/10.1080/07038992.2016.1220829>, 2016.

Mensah, S., Glèlè Kakai, R., and Seifert, T.: Patterns of biomass allocation between foliage and woody structure: the effects of tree size and specific functional traits, *Ann. For. Res.*, 59, <https://doi.org/10.15287/afr.2016.458>, 2016.

Nguyen, V.-T., Fournier, R. A., Côté, J.-F., and Pimont, F.: Estimation of vertical plant area density from single return terrestrial laser scanning point clouds acquired in forest environments, *Remote Sensing of Environment*, 279, 113115, <https://doi.org/10.1016/j.rse.2022.113115>, 2022.

Owen, H. J. F., Flynn, W. R. M., and Lines, E. R.: Competitive drivers of inter-specific deviations of crown morphology from theoretical predictions measured with Terrestrial Laser Scanning, *J. Ecol.*, 109, 2612–2628, <https://doi.org/10.1111/1365-2745.13670>, 2021.

Owen, H. J. F., Flynn, W. R. M., and Lines, E. R.: Individual TLS tree clouds collected from both Alto Tajo and Cuellar in Spain., 10.5281/zenodo.6962717, 2022.

Peppe, D. J., Royer, D. L., Cariglino, B., Oliver, S. Y., Newman, S., Leight, E., Enikolopov, G., Fernandez-Burgos, M., Herrera, F., Adams, J. M., Correa, E., Currano, E. D., Erickson, J. M., Hinojosa, L. F., Hoganson, J. W., Iglesias, A., Jaramillo, C. A., Johnson, K. R., Jordan, G. J., Kraft, N. J. B., Lovelock, E. C., Lusk, C. H., Niinemets, Ü., Peñuelas, J., Rapson, G., Wing, S. L., and Wright, I. J.: Sensitivity of leaf size and shape to climate: global patterns and paleoclimatic applications, *New Phytol.*, 190, 724–739, <https://doi.org/10.1111/j.1469-8137.2010.03615.x>, 2011.

Pimont, F., Allard, D., Soma, M., and Dupuy, J.-L.: Estimators and confidence intervals for plant area density at voxel scale with T-LiDAR, *Remote Sensing of Environment*, 215, 343–370, <https://doi.org/10.1016/j.rse.2018.06.024>, 2018.

Pimont, F., Soma, M., and Dupuy, J.-L.: Accounting for Wood, Foliage Properties, and Laser Effective Footprint in Estimations of Leaf Area Density from Multiview-LiDAR Data, *Remote Sensing*, 11, 1580, <https://doi.org/10.3390/rs11131580>, 2019.

Soma, M., Pimont, F., Durrieu, S., and Dupuy, J.-L.: Enhanced Measurements of Leaf Area Density with T-LiDAR: Evaluating and Calibrating the Effects of Vegetation Heterogeneity and Scanner Properties, *Remote Sensing*, 10, 1580, <https://doi.org/10.3390/rs10101580>, 2018.

Soma, M., Pimont, F., Allard, D., Fournier, R., and Dupuy, J.-L.: Mitigating occlusion effects in Leaf Area Density estimates from Terrestrial LiDAR through a specific kriging method, *Remote Sensing of Environment*, 245, 111836, <https://doi.org/10.1016/j.rse.2020.111836>, 2020.

Vicari, M. B., Disney, M., Wilkes, P., Burt, A., Calders, K., and Woodgate, W.: Leaf and wood classification framework for terrestrial LiDAR point clouds, *Methods Ecol. Evol.*, 10, 680–694, <https://doi.org/10.1111/2041-210X.13144>, 2019.

Wan, P., Shao, J., Jin, S., Wang, T., Yang, S., Yan, G., and Zhang, W.: A novel and efficient method for wood–leaf separation from terrestrial laser scanning point clouds at the forest plot level, *Methods in Ecology and Evolution*, 12, 2473–2486, <https://doi.org/10.1111/2041-210X.13715>, 2021.

Wang, D.: Unsupervised semantic and instance segmentation of forest point clouds, *ISPRS Journal of Photogrammetry and Remote Sensing*, 165, 86–97, <https://doi.org/10.1016/j.isprsjprs.2020.04.020>, 2020.

Wang, D., Brunner, J., Ma, Z., Lu, H., Hollaus, M., Pang, Y., and Pfeifer, N.: Separating Tree Photosynthetic and Non-Photosynthetic Components from Point Cloud Data Using Dynamic Segment Merging, *Forests*, 9, 252, <https://doi.org/10.3390/f9050252>, 2018.

Wang, D., Momo Takoudjou, S., and Casella, E.: LeWoS: A universal leaf-wood classification method to facilitate the 3D modelling of large tropical trees using terrestrial LiDAR, *Methods Ecol Evol*, 11, 376–389, <https://doi.org/10.1111/2041-210X.13342>, 2020.

Wilkes, P., Lau, A., Disney, M., Calders, K., Burt, A., Gonzalez de Tanago, J., Bartholomeus, H., Brede, B., and Herold, M.: Data acquisition considerations for Terrestrial Laser Scanning of forest plots, *Remote Sens. Environ.*, 196, 140–153, <https://doi.org/10.1016/j.rse.2017.04.030>, 2017.

Wu, B., Zheng, G., and Chen, Y.: An Improved Convolution Neural Network-Based Model for Classifying Foliage and Woody Components from Terrestrial Laser Scanning Data, *Remote Sensing*, 12, 1010, <https://doi.org/10.3390/rs12061010>, 2020.

You, H., Li, S., Ma, L., and Wang, D.: Leaf Area Index Retrieval for Broadleaf Trees by Envelope Fitting Method Using Terrestrial Laser Scanning Data, *IEEE Geoscience and Remote Sensing Letters*, 19, 1–5, <https://doi.org/10.1109/LGRS.2022.3214427>, 2022.



# Quantifying vegetation indices using Terrestrial Laser Scanning: methodological complexities and ecological insights from a Mediterranean forest

William Rupert Moore Flynn<sup>1</sup>, Harry Jon Foord Owen<sup>2</sup>, Stuart William David Grieve<sup>1,3</sup> and Emily Rebecca Lines<sup>2</sup>

<sup>1</sup>School of Geography, Queen Mary University of London, Mile End Rd, Bethnal Green, London E1 4NS

<sup>2</sup>Department of Geography, University of Cambridge, Downing Place, Cambridge, CB2 3EN

<sup>3</sup>Digital Environment Research Institute, Queen Mary University of London, New Road, London, E1 1HH

Correspondence to: W. R. M. Flynn ([w.r.m.flynn@qmul.ac.uk](mailto:w.r.m.flynn@qmul.ac.uk))

**Abstract.** Accurate measurement of vegetation density metrics including plant, wood and leaf area indices (PAI, WAI and LAI) is key to monitoring and modelling carbon storage and uptake in forests. Traditional passive sensor approaches, such as Digital Hemispherical Photography (DHP), cannot separate leaf and wood material, nor individual trees, and require many assumptions in processing. Terrestrial Laser Scanning (TLS) data offer new opportunities to improve understanding of tree and canopy structure. Multiple methods have been developed to derive PAI and LAI from TLS data, but there is little consensus on the best approach, nor are methods benchmarked as standard.

Using TLS data collected in 33 plots containing 2472 trees of five species in Mediterranean forests, we compare three TLS methods (*LiDAR Pulse*, *2D Intensity Image* and *Voxel-Based*) to derive PAI and compare with co-located DHP. We then separate leaf and wood in individual tree point clouds to calculate wood to total plant area ( $\alpha$ ), a metric to correct for non-photosynthetic material in LAI estimates. We use individual tree TLS point clouds to estimate how  $\alpha$  varies with species, tree height and stand density.

We find the *LiDAR Pulse* method agrees most closely with DHP, but is limited to single scan data so cannot determine individual tree  $\alpha$ . The *Voxel-Based* method shows promise for ecological studies as it can be applied to individual tree point clouds. Using the *Voxel-Based* method, we show that species explain some variation in  $\alpha$ , however, height and density were ~~stronger~~ better predictors.

Our findings highlight the value of TLS data to improve fundamental understanding of tree form and function, but also the importance of rigorous testing of TLS data processing methods at a time when new approaches are being rapidly developed. New algorithms need to be compared against traditional methods, and existing algorithms, using common reference data. Whilst promising, our results show that metrics derived from TLS data are not yet reliably calibrated and validated to the extent they are ready to replace traditional approaches for large scale monitoring of PAI and LAI.

## 1 Introduction

Terrestrial Laser Scanning (TLS) generates high-resolution 3D measurements of whole forests and individual trees (Burt et al., 2018; Disney, 2018), leading to the development of completely new monitoring approaches to understand the structure and function of ecosystems (Lines et al., 2022). Unlike traditional passive sensors, TLS can estimate plant, wood and leaf area indices (PAI; WAI; LAI) for both whole plots and individual tree point clouds (Calders et al., 2018), and is unaffected by illumination conditions. This has led to the development of several methods for processing TLS data to extract the key metrics PAI, WAI and LAI (e.g. Hosoi and Omasa, 2006; Jupp et al., 2008; Zheng et al., 2013). However, intercomparison of algorithms and processing approaches to derive the same metrics from different TLS methods are lacking.

Leaf Area Index (LAI), defined as half the amount of green leaf area per unit ground area (Chen and Black, 1992), determines global evapotranspiration, phenological patterns and canopy photosynthesis, and is therefore an essential climate variable (ECV), as well as a key input in dynamic global vegetation models (Sea et al., 2011; Weiss et al., 2004). Accurate measurements of LAI, WAI and PAI have historically been derived from labour intensive destructive sampling (Baret et al., 2013; Jonckheere et al., 2004), so over large spatial or temporal scales these can only be measured indirectly, typically with remote sensing. Large-scale remote sensing, using spaceborne and airborne instruments, has been widely used to estimate LAI over large areas (Pfeifer et al., 2012), but requires calibration and validation using in situ measurements to constrain information retrieval (Calders et al., 2018). Non-destructive in situ vegetation index estimates have historically been made by measuring light transmission below the canopy and using simplifying assumptions about canopy structure to estimate the amount of intercepting material (e.g. Beer-Lambert law; Monsi and Saeki, 1953). The most common method, Digital Hemispherical photography (DHP; Figure 1a), requires both model assumptions and subjective user choices during data acquisition and processing in order to estimate both PAI and LAI (Breda, 2003). DHP images are processed by separating sky from canopy, but not photosynthetic from non-photosynthetic vegetative material, so additional assumptions are needed to calculate either LAI or WAI (Jonckheere et al., 2004; Pfeifer et al., 2012). Separation of LAI from PAI can be achieved by removing or masking branches and stems from hemispherical images (e.g. Sea et al., 2011; Woodgate et al., 2016), but is not reliable when leaves are occluded by woody components (Hardwick et al., 2015). An alternative approach is to take separate DHP measurements in both leaf on and leaf off conditions, and derive empirical wood to plant ratios (WAI/PAI,  $\alpha$ ) (Leblanc and Chen, 2001), but this is not always practical, for example in evergreen forests. The difficulty of separation means that studies often omit correcting for the effect of WAI on optical PAI measurements altogether (Woodgate et al., 2016), but since woody components in the forest canopy can account for more than 30% of PAI (Ma et al., 2016) this can introduce overestimation. Further, although DHP estimates of LAI or PAI are valuable both for ecosystem monitoring and developing satellite LAI products (Hardwick et al., 2015; Pfeifer et al., 2012), they are limited to sampling only at a neighbourhood or plot level (Weiss et al., 2004), and cannot be used to measure individual tree LAI except for open grown trees (Béland et al., 2014).

The ratio of wood to total plant area,  $\alpha$ , is known to be dynamic, changing in response to abiotic and biotic conditions. For example, the Huber value (sapwood to leaf area ratio, a related measure to  $\alpha$ ) may vary according to water availability (Carter and White 2009). Leaf area may therefore be indicative of the drought tolerance level of a tree, with more drought tolerant species displaying a lower leaf area, reducing the hydraulic conductance of

the whole tree and therefore increasing its drought tolerance (Niinemets and Valladares, 2006).  $\alpha$  has been hypothesised to increase with the size of a tree in response to the increased hydraulic demand associated with greater hydraulic resistance of tall trees (Magnani et al., 2000) and higher transpiration rates of larger LAI (Battaglia et al., 1998; Phillips et al., 2003). Stand density may also impact  $\alpha$  (Long and Smith, 1988; Whitehead, 1978), as increased stand level water use scales linearly with LAI (Battaglia et al., 1998; Specht and Specht, 1989), reducing water availability to individual trees competing for the same resources (Jump et al., 2017). Large scale quantification of  $\alpha$  or Huber value, however, is difficult as studies usually rely on a small number of destructively sampled trees (e.g. Carter and White, 2009; Magnani et al., 2000), litterfall traps (e.g. Phillips et al., 2003) or masking hemispherical images (e.g. Sea et al., 2011; Woodgate et al., 2016). These approaches are only applicable on a small to medium scale, and in the case of image masking, cannot differentiate between individuals. Variation in  $\alpha$ , for example by species and or stand structure, is therefore largely unknown.

## 1.2 TLS methods for calculating PAI, LAI and WAI

TLS methods for extracting PAI, LAI and WAI can be broadly categorised into two types: (1) LiDAR return counting, using single scan data (e.g., the *LiDAR Pulse* method; Jupp et al., 2008, and *2D Intensity Image* method; Zheng et al., 2013) and (2) point cloud voxelisation, usually using co-registered scans (e.g., the *Voxel-Based* method; Hosoi and Omasa, 2006).

The *LiDAR Pulse* method (Jupp et al., 2008; Figure 1b) estimates gap fraction ( $P_{gap}$ ) using single scan data, as a function of the total number of outgoing LiDAR pulses from the sensor and the number of pulses that are intercepted by the canopy. This method, which eliminates illumination impacts associated with the use of DHP (Calders et al., 2014), has been implemented in the python module, *PyLidar* ([www.py lidar.org](http://www.py lidar.org)) and the R package, *rTLS* (Guzman, et al. 2021). Using the *LiDAR Pulse* method, Calders et al. (2018) compared TLS PAI PAI estimates from two ground-based passive sensors (LiCOR LAI-2000 and DHP) with TLS data collected with a RIEGL VZ-400 TLS in a deciduous woodland, and found the two passive sensors underestimated PAI values compared to TLS, with differences dependent on DHP processing and leaf on/off conditions.

The *2D Intensity Image* method (Zheng et al., 2013; Figure 1c), also uses raw single scan TLS point clouds, but unlike the *LiDAR Pulse* method, this approach converts LiDAR returns into 2D panoramas where pixel values represent intensity. PAI is estimated by classifying pixels as sky or vegetation, based on their intensity value, to estimate  $P_{gap}$ , and then applying Beer-Lambert's law. As for the *LiDAR Pulse* method, this approach has been shown to generate higher PAI estimates than DHP (Calders et al., 2018; Woodgate et al., 2015; Grotti et al., 2020), with differences attributed to the greater pixel resolution and viewing distance of TLS resolving more small canopy details (Grotti et al., 2020).

The *Voxel-Based* method (Figure 1d) estimates PAI by segmenting a point cloud into voxels and either simulating radiative transfer within each cube (Béland et al., 2014; Kamoske et al., 2019), or classifying voxels as either containing vegetation or not, and dividing vegetation voxels by the total number of voxels (Hosoi and Omasa, 2006; Itakura and Hosoi, 2019; Li et al., 2017). Crucially, this method may be applied to multiple co-registered scan point clouds and so can be used to calculate PAI for both whole plots and individual, segmented TLS trees.

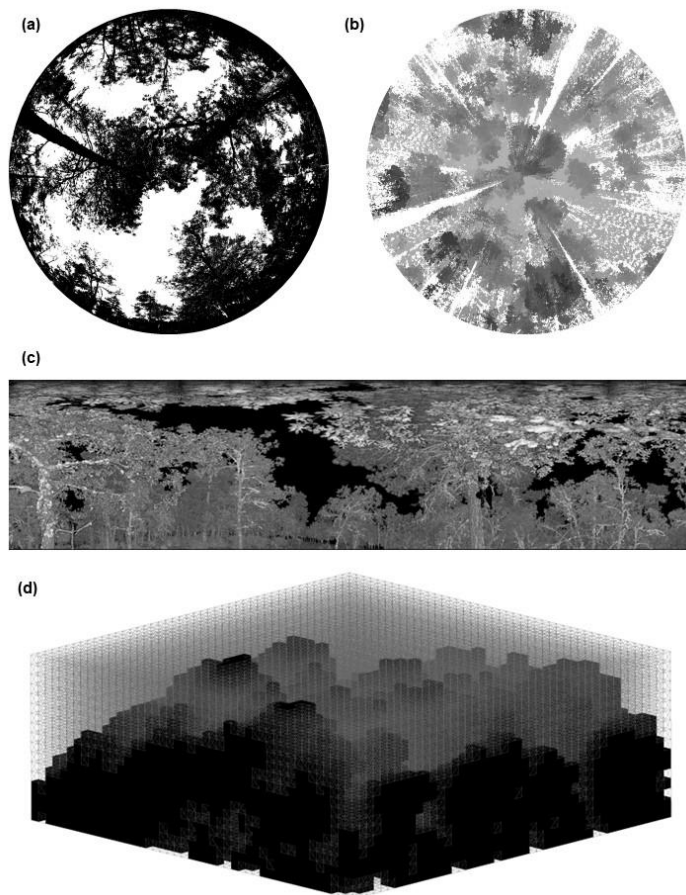
However, PAI estimates derived using the voxel method are highly dependent on voxel size (Calders et al., 2020). Using a radiative transfer approach, Béland et al., (2014) demonstrated that voxel size is dependent on canopy

Formatted: Font: 10 pt

Formatted: Font: 10 pt

clumping, radiative transfer model assumptions and occlusion effects, making a single, fixed choice of voxel size within methods for all datasets impossible. To test various approaches to selecting voxel size using a voxel classification approach, (Li et al., (2016) matched voxel size to point cloud resolution, individual tree leaf size, and minimum beam distance and tested against destructive samples, finding that voxel size matched to point cloud resolution had the closest PAI values to destructive samples.

The *LiDAR Pulse* method and *2D Intensity Image* method both use single scan data. However, to generate robust estimates of canopy properties that avoid errors from occlusion effects, multiple co-registered scans taken from different locations are likely needed (Wilkes et al., 2017). Further, both these methods require raw unfiltered data to accurately measure the ratio of pulses emitted from the scanner and number of pulses that are intercepted by vegetation. This means “noisy” points caused by backscattered pulses (Wilkes et al., 2017) are included in analyses, potentially leading to higher PAI estimates. However, the *LiDAR Pulse* and *2D Intensity Image* methods may introduce fewer estimation errors compared DHP, which is influenced by differences in sky illumination conditions and camera exposure (Weiss et al., 2004).



Formatted: Font: Not Italic

124

125 **Figure 1: Methods for PAI estimation applied in this study: (a) a binarised digital hemispherical photograph (DHP),**  
126 **(b) TLS raw single scan point cloud, used within the LiDAR Pulse method (Jupp et al., 2008). Image shows a top-down**  
127 **view of raw point cloud and greyscale represents low (grey) and high (black) Z values, (c) TLS 2D intensity image for**  
128 **the 2D Intensity Image method (Zheng et al., 2013), (d) Voxelised co-registered whole plot point cloud for the Voxel-**  
129 **Based method (Hosoi and Omasa, 2006), showing a representative schematic of cube voxels with edge length of 1m,**  
130 **voxelised using the R package VoxR (Lecigne et al., 2018). Solid black voxels are classified as containing vegetation**  
131 **(filled) and voxels outlined with grey lines are voxels classified as empty.**

Formatted: Font: Not Bold

### 132 1.3 Scope and aims

133 The aims of this study are twofold: the first aim is to compare three TLS methods for estimating PAI with  
134 traditional DHP. The second aim of this study is to use TLS to drivers of individual tree  $\alpha$  variation.

Formatted: Font: Not Bold

135 In this study we use a dataset of 528 co-located DHP and high-resolution TLS scans from 33 forest plots to  
136 compare DHP derived PAI ( $PAI_{DHP}$ ) with estimates from three methods to estimate PAI from TLS data ( $PAI_{TLS}$ ):  
137 the *LiDAR Pulse* method; the *2D Intensity Image* method and the *Voxel-Based* method (Figure 1). We use a dataset  
138 collected from a network of pine/oak forest plots in Spain (Owen et al., 2021) and ask (1) are the three TLS  
139 methods able to reproduce  $DHP-PAI_{DHP}$  estimates at single scan and whole plot level? (2) does  $\alpha$ , calculated  
140 from the *Voxel-Based* method on individual tree point clouds, vary with species and tolerance to drought; and (3)  
141 does  $\alpha$  scale with height and stand density?

Formatted: Subscript

## 142 2. Methods

### 143 2.1 Study site

144 We collected TLS and DHP data from 29 plots in Alto Tajo Natural Park ([40°41'N 02°03'W](#); FunDIV ([Functional](#)  
145 [Diversity](#)) plots; [see Baeten et al., \(2013\) for detailed description of plots](#)) and four plots in Cuellar  
146 ([41°23'N 4°21'W](#)) in June - July 2018 (see Owen et al., (2021) for full details) ([Figure B1](#)). Plots contained two  
147 oak species: semi-deciduous *Q. faginea* and evergreen *Q. ilex*, and three pine species: *P. nigra*, *P. pinaster* and *P.*  
148 *sylvestris*. *P. sylvestris* is the least drought tolerant species, followed by *P. nigra*, *Q. faginea*, *Q. ilex*; shade  
149 tolerance follows the same ranking (Niinemets and Valladares, 2006; Owen et al., 2021). Although not  
150 quantitatively ranked, *P. pinaster* has been shown to be very drought tolerant, appearing in drier areas than the  
151 other species (Madriral-González et al., 2017). The area is characterised by a Mediterranean climate (altitudinal  
152 [gradient range](#) 840 – 1400 m.a.s.l.) (Jucker et al., 2014; Madriral-González et al., 2017). In addition to the five  
153 main canopy tree species, plots contained an understory of *Juniperus thurifera* and *Buxus sempervirens* (Kuusk  
154 et al., 2018).

### 155 2.2 Field protocol

156 In each of the 33 30 x 30 m plots we collected TLS scans on a 10 m grid, making 16 scan locations following  
157 Wilkes et al., (2017) to minimise occlusion effects associated with insufficient scans. We used a Leica HDS6200  
158 TLS set to super high resolution (3.1 x 3.1 mm resolution at 10 m with a beam divergence of  $\leq 5$  mm at 50 m; scan  
159 time 6m 44 s; see Owen et al., (2021)). At each of the 528 scan locations and following the protocol in Pfeifer et  
160 al., (2012), we captured co-located DHP images with three exposure settings (automatic and  $\pm$  one stop exposure  
161 compensation), levelling a Canon EOS 6D full frame DSLR sensor with a Sigma EX DG F3.5 fisheye lens,  
162 mounted on a Vanguard Alta Pro 263AT tripod.

### 2.3 Calculation of single scan and whole plot PAI using DHP data

For each of the red-green-blue (RGB) DHP images we extracted the blue band for image thresholding, as this best represents sky/vegetation contrast (Pfeifer et al., 2012). For each plot, we picked the exposure setting that best represented sky/vegetation difference based on pixel brightness histograms of four sample locations indicative of the plot. We carried out automatic image thresholding using the Ridler and Calvard method (1978), to create a binary image of sky and vegetation, avoiding subjective user pixel classification (Jonckheere et al., 2005). We calculated PAI from the binary image, limiting the field of view to a 5° band centred on the hinge angle of 57.5° (55° – 60°). The hinge angle has a path length through the canopy twice the canopy height, so the band around it is an area of significant spatial averaging taken as representative of canopy structure of the area (Calders et al., 2018; Jupp et al., 2008). From the binarised hinge angle band we calculated  $\text{gap-fraction}P_{\text{gap}}$  as the number of sky pixels divided by the total number of pixels and PAI using an inverse Beer-Lambert law equation (Monsi and Saeki, 1953). We calculated whole plot PAI as the arithmetic mean within plot scan location PAI. As this value does not correct for canopy clumping, it is better described as effective PAI, rather than true PAI (Woodgate et al., 2015). However, as the TLS and DHP methods we apply here account for canopy clumping differently, we compared effective values and here-on refer to effective PAI as PAI (Calders et al., 2018).

### 2.4 Calculation of single scan and whole plot PAI from TLS data

To calculate PAI using the *LiDAR Pulse* method (Jupp et al., 2008), we calculated the  $\text{gap-fraction}(P_{\text{gap}})$  for a single scan (Figure 1b) by summing all returned laser pulses and dividing by the number of total outgoing pulses, following Lovell et al. (2011; see Eq. 7 in that study), and then estimated PAI following Jupp et al. (2008; see Eq. 18 in that study), setting the sensor range to 5° around the hinge angle as before (55° – 60°). Single scan PAI was taken as the cumulative sum of PAI values estimated by vertically dividing the hinge region into 25 cm intervals (Calders et al., 2014). We implemented the *LiDAR Pulse* method using the open-source *R* (R Core Team, 2020) package, *rTLS* (Guzmán and Hernandez, 2021).

To calculate PAI using the *2D Intensity Image* method (Zheng et al., 2013), we converted 3D TLS point cloud data from all 528 scan locations into polar coordinates, and scaled intensity values to cover the full 0-255 range (Figure 1c) and rasterised into a 2D intensity image using the open-source *R* package, *raster* (Hijmans, 2022). We cut the 2D intensity image to a 5° band around the hinge angle (55° – 60°) and classified sky and vegetation pixels in each image using the Ridler and Calvard method (1978). We calculated  $P_{\text{gap}}$  as the number of pixels classified as sky divided by the total number of pixels and derived PAI with an inverse Beer-Lambert law equation (Monsi and Saeki, 1953).

Following the same approach as applied to our DHP data, we calculated whole plot PAI for the *LiDAR Pulse* and *2D Intensity Image* methods as the arithmetic mean of within plot single scan PAI estimates.

To calculate PAI using the *Voxel-Based* method, we followed a voxel classification approach (Hosoi and Omasa, 2006), downsampling the point cloud to 0.05 m to aid computation time and matching the voxel size to the resolution of the point cloud (0.05 m), following (Li et al., 2016), who showed that matching the voxel size to the point cloud point to point minimum distance (resolution) increases accuracy as small canopy gaps are not included in voxels classified as vegetation. We chose a voxel classification approach as this method is widely applicable to a range of TLS systems and levels of processing as well as providing explicit guidance on voxel size

Formatted: Subscript

Formatted: Subscript

selection, which is known to impact derived PAI estimates (Li et al., 2016). We re-combined individually segmented trees, filtered for noise using a height-dependent statistical filter (see Owen et al., 2021) back into whole plot point clouds and voxelised them using the open source R package, VoxR (Lecigne et al., 2018), with a full grid covering the minimum to maximum XYZ ranges of the plot. We classified any voxel containing > 0 points as vegetation (“filled”), and empty voxels as gaps. We then split the voxelised point cloud into slices one voxel high. Within each slice, the contact frequency is calculated as the fraction of filled to total number of voxels. We then multiplied the contact frequency by a correction factor for leaf inclination, set at 1.1 (Li et al., 2017), and whole plot PAI was calculated as the sum of all slices’ contact frequencies.

## 2.5 Calculation of individual tree PAI, WAI and $\alpha$ using the voxel-based method

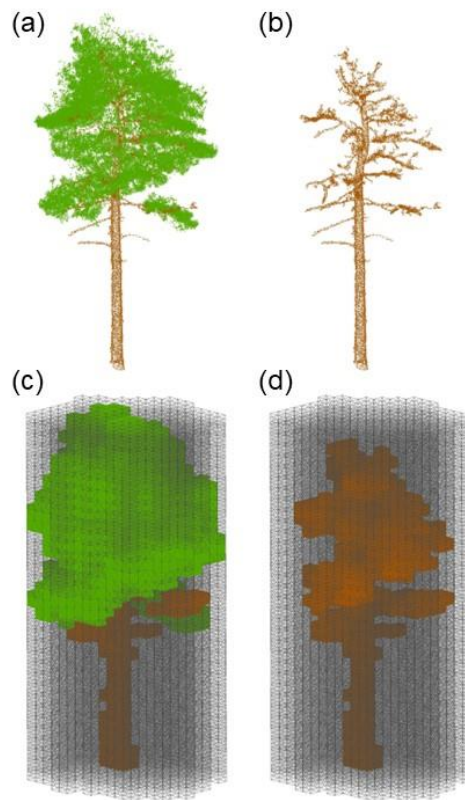


Figure 2: Visualisation of the workflow for applying the Voxel-Based method to estimate individual-tree PAI, WAI and  $\alpha$ . (a) Individual tree point cloud; (b) separated leaf off (wood) individual tree point cloud; (c) voxelised individual tree point cloud; (d) voxelised wood cloud. Solid black-Coloured voxels (green represents leaf and brown represents wood) are filled voxels and grey lines are empty voxels. Empty voxels occupy the space within the projected crown area of the tree. Image shows schematic of point cloud voxelised with cube voxels with edge length of 0.5 m. Panels a and b show wood and leaf separation of an example *P. sylvestris*, was carried out using *TLSeparation* (Vicari et al., 2019). Point cloud voxelisation was carried out using modified functions from R package *VoxR* (Lecigne et al., 2018).



As the only method using multiple co-registered scans, the *Voxel-Based* method is only method compared in this study we found capable of deriving PAI, WAI and LAI of segmented individual tree point clouds estimating individual tree leaf and wood properties. We estimated PAI and WAI for 2472 individual trees segmented from co-registered point clouds following a similar method to the whole plot point cloud. We used individual tree point clouds downsampled to 0.05 m, to aid computation time, and extracted segmented individual trees using the automated tree segmentation program *treeseq* (Burt et al., 2019), implemented in C++, see by Owen et al., (2021) for that study, full details, and Individual segmented tree data are available in Owen et al., (2022), for individual segmented tree data.

To estimate PAI, WAI and  $\alpha$  for each tree, we first separated leaf from wood points in used individual tree point clouds wood – leaf separated by (Owen et al., (2021) using the open source Python library *TLSeparation* (Vicari et al., 2019), and then used the separated wood-only point clouds to calculate WAI. *TLSeparation* classifies assigns points as as either leaf or wood, iteratively looking at a predetermined number of nearest neighbours (*knn*). The *knn* of each iteration is directly dependent on point cloud density, since high density point clouds will require higher a *knn* (Vicari et al., 2019). We used the utility package in *TLSeparation* was used to automatically detect the optimum *knn* for each tree point cloud.

To voxelise individual tree complete (Figure 2a) and wood only (Figure 2b) point clouds, we used a modified approach based on Lecigne et al., (2018), voxelising within the projected crown area of the whole tree point cloud (Figure 2c) to calculate PAI. In the same way as for PAI, we calculated WAI using the separated wood point cloud within the projected crown area of the whole tree (Figure 2d; using the whole crown and not just the wood point cloud), and derived  $\alpha$  for each tree as  $WAI/PAI$ . To allow a comparison with existing literature estimating  $\alpha$ , (Sea et al., 2011; Woodgate et al., 2016) we focused on  $\alpha$  values.

## 2.6 Statistical Analyses

We tested the relationships between  $PAI_{TLS}$  and  $PAI_{DHP}$  estimates using Standardised Major Axis (SMA) using the open source *R* (R Core Team, 2020) package, *smatr* (Warton et al., 2012). SMA is an approach to estimating a line of best fit where we are not able to predict one variable from another (Warton et al., 2006); we chose SMA because we do not have a ‘true’ validation dataset, so avoid assuming either DHP or any of the TLS methods produces the most accurate results. For each TLS method, we assessed the relationship with DHP using the coefficient of determination and RMSE. We chose to compare PAI values rather than WAI or LAI as each method corrects for non-photosynthetic elements in different ways and would introduce bias, limiting the ability to directly compare metrics. To further understand observed drivers of variance in PAI, we tested the relationship between PAI and TLS estimated whole plot crown area index, CAI, calculated as the sum of projected crown area, divided by the plot area (Owen et al., 2021), and indicative and a proxy measure of stand density and local competition (Caspersen et al., 2011; Coomes et al., 2012), using SMA.

To test if  $\alpha$  differs by species, we used linear mixed models (LMMs) in the *R* package, *lme4* (Bates et al., 2015). We included an intercept only random plot effect to account for local effects on  $\alpha$ :

$$\alpha_{i,s,j} = a_s + Plot_j \quad (1)$$

Formatted: Subscript

Formatted: Subscript



254

255 here,  $\alpha_i$  is  $\alpha$  of an individual of species  $s$ , in plot  $j$ , and  $a_s$  is the parameter to be fit. To test the effect of stand  
256 structure and tree height on  $\alpha_s$  we fit relationships separately for each species, again including a random plot  
257 effect:

258

259 
$$\alpha_{i,s,j} = a_s + b_s H_i + c_s CAI_j + Plot_{s,j} \quad (2)$$

260

261 here  $H_i$  is the height of the tree,  $CAI_j$  is the crown area index for the plot, with other parameters as before.

262 For each species' model (equation 2), we calculated the intra-class correlation coefficient (ICC). The ICC, similar  
263 to coefficient of determination, quantifies the amount of variance explained by the random effect in a linear mixed  
264 model (Nakagawa et al., 2017).

### 265 3. Results

#### 266 3.1 Comparison of plant area index estimated by DHP and single scan TLS

267 Of the two single scan TLS methods tested (*LiDAR Pulse* method and *2D Intensity Image* method), we found that  
268 ~~the relationship between~~ PAI estimated using the *LiDAR Pulse* method ~~and more strongly agreed with DHP~~  
269 ~~PAI PAI<sub>DHP</sub>, but there was also significant correlation for had a higher  $R^2$  than~~ the *2D Intensity Image* method  
270 (SMA; *LiDAR Pulse* method  $R^2 = 0.50$ , slope = 0.73,  $p < 0.001$ , RMSE = 0.14, and *2D Intensity Image* method  $R^2$   
271 = 0.22, slope = 0.38,  $p < 0.001$ , RMSE = 0.39, respectively, Figure 3a). At larger PAI values, ~~relative to DHP~~, both  
272 TLS methods underestimated PAI ~~compared with DHP~~ (Figure 3b). We found statistically significant negative  
273 correlations between residuals and DHP for both methods (SMA; *2D Intensity Image* method residuals  $R^2 = 0.85$ ,  
274 slope = -0.88,  $p < 0.01$ ; *LiDAR Pulse* method residuals  $R^2 = 0.47$ , slope = -0.70,  $p < 0.01$ ; Figure 3b). The *2D*  
275 *Intensity Image* method showed larger underestimation at higher ~~DHP PAI PAI<sub>DHP</sub>~~ values, suggesting this method  
276 may saturate sooner than both DHP and the *LiDAR Pulse* method at higher PAI values (Figure 3b).

Formatted: Subscript

Formatted: Superscript

Formatted: Subscript

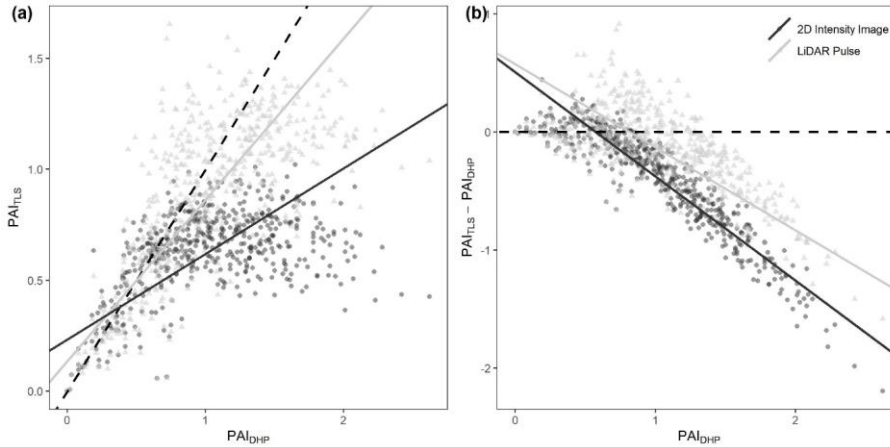


Figure 3: Comparison of single scan  $\text{TLS PAI}_{\text{TLS}}$  and  $\text{DHP PAI}_{\text{DHP}}$  estimates, for all 528 scan locations (16 per plot). (a) The correlation between DHP derived PAI with PAI derived using the 2D Intensity Image method  $R^2 = 0.22$ , slope = 0.38,  $p < 0.001$ , RMSE = 0.39 (circles), and LiDAR Pulse method  $R^2 = 0.50$ , slope = 0.73,  $p < 0.001$ , RMSE = 0.14 (triangles). Dashed line in panel a represents 1:1 relationship. (b) The difference between  $\text{TLS PAI}_{\text{TLS}}$  and  $\text{DHP PAI}_{\text{DHP}}$  estimates for the 2D Intensity Image method, and LiDAR Pulse method (dashed line at in panel b represents 0). Lines show statistically significant relationships fitted using SMA ( $p < 0.01$ ).

### 3.2 Comparison of whole plot plant area index estimated using TLS and DHP and the effect of plot structure on PAI

We found statistically significant correlations between whole plot  $\text{TLS whole plot PAI}_{\text{TLS}}$  values and  $\text{DHP PAI}_{\text{DHP}}$  for all three TLS methods. As for single scans (Figure 3), the LiDAR Pulse method showed the closest agreement to  $\text{DHP PAI}_{\text{DHP}}$ , here compared to both the Voxel-Based and 2D Intensity Image methods (SMA; LiDAR Pulse method  $R^2 = 0.66$ , slope = 0.82,  $p < 0.01$ , RMSE = 0.14; Voxel-Based method  $R^2 = 0.39$ , slope = 2.76,  $p < 0.01$ , RMSE = 0.88; 2D Intensity Image method  $R^2 = 0.35$ , slope = 0.36,  $p < 0.01$ , RMSE = 0.39, respectively; Figure 4a). The 2D Intensity Image method and LiDAR Pulse method consistently underestimated PAI compared to DHP, whilst the Voxel-Based method underestimated in plots with lower  $\text{DHP PAI}_{\text{DHP}}$  and overestimated in plots with higher  $\text{DHP PAI}_{\text{DHP}}$ . The Voxel-Based method's high PAI values compared to other methods is likely due to its use of multiple co-registered scans reducing occlusion effects prevalent in single scan data.

To assess the effect of plot structure on variation in TLS derived PAI, we compared  $\text{TLS PAI}_{\text{TLS}}$  estimates to TLS estimated crown area index (CAI,  $\text{m}^2$  projected crown area per  $\text{m}^2$  ground area, Figure 4b). We found a significant positive relationship between CAI and PAI estimated using each of the LiDAR Pulse method, the Voxel-Based method, and DHP (SMA; LiDAR Pulse method  $R^2 = 0.79$ , slope = 1.69,  $p < 0.01$ ; Voxel-Based method  $R^2 = 0.76$ , slope = 5.72,  $p < 0.01$ ; 2D Intensity Image method  $R^2 = 0.15$ , slope = 0.76,  $p < 0.05$ ; DHP  $R^2 = 0.46$ , slope = 2.07,  $p < 0.01$ , respectively; Figure 4b), where the 2D Intensity Image method appears to saturate at medium CAI values (Figure 4b).

Formatted: Subscript

Formatted: Subscript

Formatted: Font: 9 pt, Bold

Formatted: Font: 9 pt, Bold

Formatted: Subscript

Formatted: Subscript

Formatted: Subscript

Formatted: Subscript

Formatted: Subscript

Formatted: Subscript

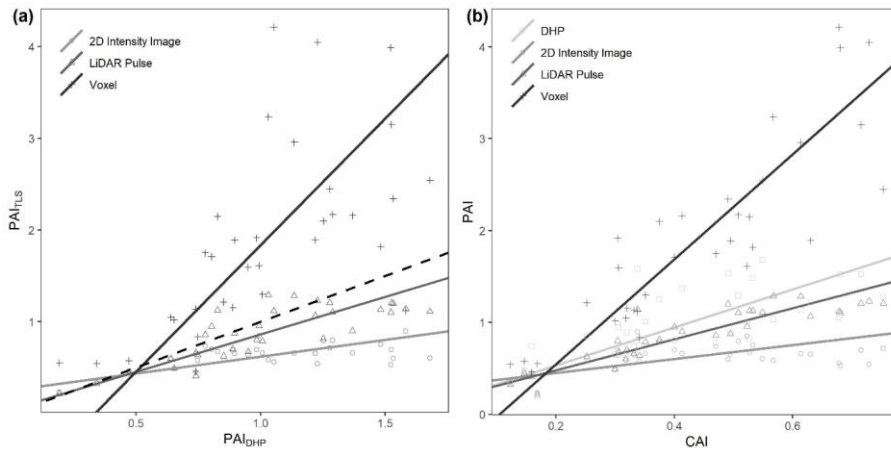


Figure 4: Comparison of plot level  $PAI_{TLS}$  and  $PAI_{DHP}$ , and CAI vs PAI estimates for all 33 plots. (a) The correlation between DHP derived PAI and PAI derived using 2D Intensity Image  $R^2 = 0.35$ , slope = 0.36,  $p < 0.01$ , RMSE = 0.39 (circle), LiDAR Pulse  $R^2 = 0.66$ , slope = 0.82,  $p < 0.01$ , RMSE = 0.14 (triangle) and Voxel-Based  $R^2 = 0.39$ , slope = 2.76,  $p < 0.01$ , RMSE = 0.88 (cross) methods (b) The correlation between TLS derived CAI and PAI derived using DHP  $R^2 = 0.46$ , slope = 2.07,  $p < 0.01$  (square), 2D Intensity Image  $R^2 = 0.15$ , slope = 0.76,  $p < 0.05$  (circle) LiDAR Pulse  $R^2 = 0.79$ , slope = 1.69,  $p < 0.01$  (triangle) and Voxel-Based  $R^2 = 0.76$ , slope = 5.72,  $p < 0.01$  (cross) methods. Lines show statistically significant relationships fitted using SMA ( $p < 0.01$ ). Dashed line in panel a represents 1:1 relationship.

### 3.4 Influence of species, tree height and CAI on $\alpha$

To understand drivers of variance in  $\alpha$ , we used individual tree PAI and WAI, calculated using the *Voxel-Based* method to test the relationship between species and  $\alpha$ , and height/ CAI and  $\alpha$ . We found that more drought tolerant species generally had higher  $\alpha$  values than less drought tolerant species (Table A1; Figure 5), however, confidence intervals were wide and overlapping, suggesting that species is not a strong predictor of variation in  $\alpha$ . We found a statistically significant negative effect of height ( $p < 0.001$ ; Table A2; Figure 6a) and positive effect of CAI ( $p < 0.01 - 0.05$ ; Table A2; Figure 6b) on  $\alpha$  for all species apart from *P. sylvestris*.  $\alpha$  decreased more rapidly with height and increased less rapidly with CAI for oaks than pines. Statistically significant ICC values were higher for *P. nigra* (ICC = 0.211; Table A2) than *P. pinaster*, *Q. faginea* and *Q. ilex* (ICC = 0.036; 0.060; 0.070, respectively), showing that more  $\alpha$  variation is explained by the random plot effect in *P. nigra* than the other species. *P. pinaster* has a wider confidence interval (Figure 5), possibly explained by its lower sample size. To

understand drivers of variance in WAI we carried out additional analysis to test the relationship between WAI and species, height, CAI and PAI, and presented these results in Appendix C.

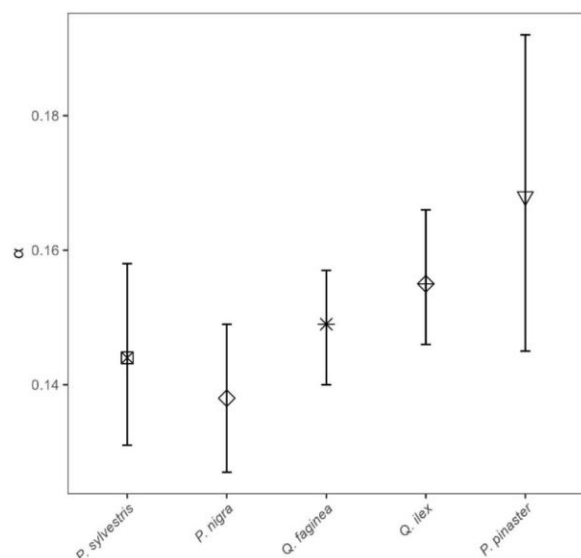


Figure 5: Linear mixed model derived  $\alpha$  values (a, equation 1) for all 2472 individual trees of species *P. sylvestris*, *P. nigra*, *Q. faginea*, *Q. ilex* and *P. pinaster*. Error bars represent 95% confidence intervals. Species are listed from low – high drought tolerance, with the exception of *P. pinaster*, for which drought tolerance index has not been calculated in the literature. Drought tolerance rankings are taken from (Niinemets and Valladares, (2006))

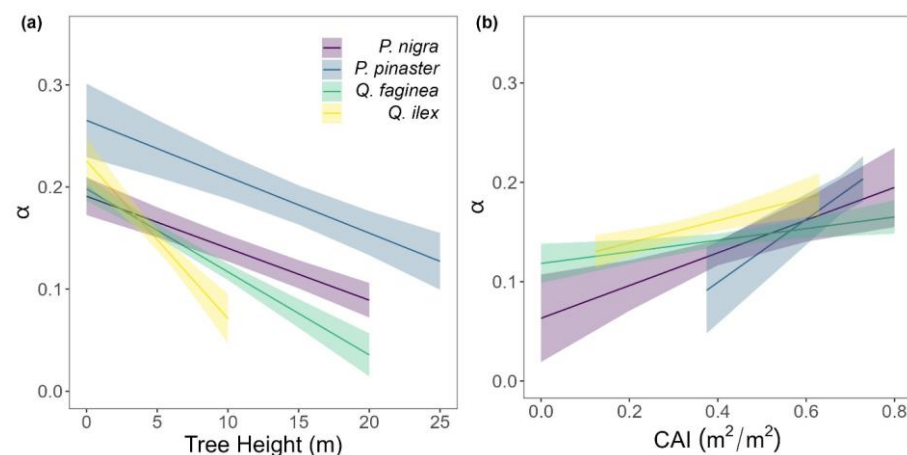


Figure 6: Variation in  $\alpha$  for each species: *Pinus nigra*, *P. pinaster*, *Q. faginea* and *Q. ilex* with (a) height and (b) plot CAI. Lines represent statistically significant linear mixed models (equation 2;  $p < 0.001$  –  $p < 0.05$ ). Ribbons represent 95% confidence intervals. The model for *P. sylvestris* was not statistically significant.

333

## 334 4. Discussion

### 335 4.1 Comparison of approaches to deriving PAI from remote sensed data

336 We found substantial differences in PAI values estimated from TLS and DHP and from different TLS processing  
337 methods (Figures 3 and 4). Further, differences between TLS methods varied across plot structure (CAI), with the  
338 greatest differences between methods in plots with high CAI, and therefore high canopy density. Although  
339 previous studies have presented TLS as an improvement over DHP due to its independence of illumination and  
340 sky conditions during the data acquisition phase, and ability to resolve fine-scale canopy elements and gaps  
341 (Calders et al., 2018; Grotti et al., 2020; Zhu et al., 2018), we have shown that there is large variability between  
342 TLS processing methods in Mediterranean forests. Rigorous intercomparison of approaches, ideally using  
343 standard benchmarking TLS datasets, and destructive sampling, would improve trust and reliability of TLS  
344 algorithms.

### 345 4.2 The LiDAR Pulse and 2D Intensity Image method derived PAI estimates were lower than those derived 346 from DHP and the Voxel-Based method

347 We found the *LiDAR Pulse* method (Jupp et al., 2008) to have the best agreement with DHP for both whole plot  
348 and single scan PAI estimates. In contrast to previous studies comparing  $PAI_{TLS}$  with  $PAI_{DHP}$  comparisons  
349 (Calders et al., 2018; Grotti et al., 2020; Woodgate et al., 2015), we found that the *LiDAR Pulse* and *2D Intensity*  
350 *Image* methods underestimated PAI compared to DHP, except at very low PAI values ( $PAI_{TLS} < 0.5$ ).  
351 Quantification of PAI from DHP may introduce additional sources of error, for example, its relatively lower  
352 resolution compared to TLS could lead to mixed pixels that have a greater chance of misclassification of sky as  
353 vegetation (Jonckheere et al., 2004). This effect could be enhanced in a Mediterranean forest as trees in drier  
354 climates tend to have smaller leaves (Peppe et al., 2011), leading to more small canopy gaps that TLS may resolve  
355 where DHP cannot. Further, although we took steps to reduce the error introduced at DHP data acquisition and  
356 processing steps, including using automatic thresholding and collecting images with multiple exposures, DHP  
357 processing requires both model and user assumptions that can impact results. For example,  $DHP-PAI/PAI_{DHP}$   
358 estimates are highly sensitive to camera exposure; increasing one stop of exposure can result in 3 – 28% difference  
359 in PAI and use of automatic exposure can result in up to 70% error (Zhang et al., 2005).

360 We found the *Voxel-Based* method overestimated PAI values compared to the other methods at the whole plot  
361 level. This is likely due to the method's use of co-registered scans, rather than averaged single scan PAI values,  
362 since co-registered scans will reduce occlusion effects prevalent in single scan data that could lead to an  
363 underestimation of PAI (Wilkes et al., 2017). The *Voxel-Based* method is, however, sensitive to voxel size (Li et  
364 al., 2016), and larger voxels lead to larger PAI estimates as they fill small canopy gaps; we chose a voxel size of  
365 0.05 m to match the minimum distance between points in our downsampled dataset. However, the *Voxel-Based*  
366 method is a memory intensive approach to calculating PAI, and smaller voxels have higher memory requirements.  
367 We picked this data resolution, and therefore voxel size, to balance the need to capture fine-scale canopy details  
368 against memory requirements for running many large plots. Voxel size could have been chosen based on  
369 estimates' match to DHP, but this would assume (1) that DHP estimates are most accurate, and (2) that DHP data  
370 are always available, limiting the wider applicability of our findings. Understanding which method is over or  
371 underestimating would require a destructively sampled dataset for validation, which was not possible for this

Formatted: Subscript

Formatted: Subscript

Formatted: Subscript

Formatted: Subscript

study (or most ecosystems). However, other studies using voxel approaches have found that although these produce high LAI values for individual trees, these are underestimates compared with destructive samples (Li et al., 2016). Regardless, PAI and LAI estimates using a *Voxel-Based* approach are highly dependent on voxel size (Béland et al., 2014) (Li et al., 2016), and future work should test the influence of voxel size on PAI estimates, using destructive samples in a range of environments.

#### 4.3 Relationship between PAI and CAI varied according to method and sensor

The relationship between the *LiDAR Pulse* method had the strongest relationship (defined as highest  $R^2$ ) with and TLS derived CAI had the highest  $R^2$ , demonstrating that the method is well suited to measuring PAI across the range of plot CAI values used in this study. Although the *2D Intensity Image* method can tackle the significant challenges presented by edge effects and partial beam interceptions, particularly present in phase-shift systems (Grotti et al., 2020), our results suggest this method has a lower performance ability, with saturation occurring sooner than all other methods in dense forests (Figures 3 and 4). The *2D Intensity Image* method uses the same raw single scan data as the *LiDAR Pulse* method, so the better performance from the latter is likely due to the method's use of vertically resolved gap fraction; both the *LiDAR Pulse* method and *Voxel-Based* method account for the vertical structure of the canopy by summing vertical slices through the canopy.

#### 4.4 $\alpha$ variation between species and plot

We used the *Voxel-Based* method to investigate individual tree  $\alpha$  variation between species and across structure, as this was the only approach we compared identified that could be applied to single tree point clouds. We found  $\alpha$  values obtained were within the range of values obtained from destructive approaches (0.1 – 0.6, Gower et al., 1997). The drought and shade intolerant *P. nigra* showed stronger variability in  $\alpha$  across plots (higher ICC value, Table A2) than other species, suggesting its wood – leaf ratio may be more sensitive to site factors. However, as the plots measured in this study vary in both abiotic conditions (altitude, aspect, slope, wetness) as well as species composition, stem density and canopy cover, there may be other drivers of variation in  $\alpha$  values.

We found some evidence that species with higher drought tolerance had higher  $\alpha$  values (Figure 5; Table A1), however, confidence intervals were wide, suggesting a weak relationship. There is evidence that trees that tolerate water limited environments have a lower leaf area (Battaglia et al., 1998; Mencuccini and Grace, 1995), so higher  $\alpha$  values may reflect maintenance of homeostasis of leaf water use through adjustment of wood to leaf area ratio (Carter and White, 2009; Gazal et al., 2006). The potential for a tree to lose water is mostly regulated through leaf traits including stomatal conductance and leaf area, and both stand (Battaglia et al., 1998; Specht and Specht, 1989) and individual tree (Mencuccini, 2003) water use have been found to scale linearly with LAI, with drought often mitigated through leaf shedding (López et al., 2021).

#### 4.5 Tree stature and stand density drives $\alpha$ variation

Although species had a weak relationship with explain some variation in  $\alpha$ , tree height and plot CAI were stronger predictors had a statistically significant relationship with  $\alpha$  ( $p < 0.001$  –  $p < 0.05$ ) for all species, showing the importance of local stand structure on leaf and woody allocation. We found that  $\alpha$  scaled negatively with height for all species apart from *P. sylvestris*, suggesting that in this environment, taller trees generally have a lower proportion of wood to plant area index than shorter ones. *P. sylvestris*, which is at the edge of its geographical range and physiological limits (Castro-Díez et al., 1997; Owen et al., 2021), showed no significant relationship

between height and  $\alpha$ . We found that  $\alpha$  scaled positively with plot level CAI for all species apart from *P. sylvestris*, that is, trees growing in denser plots have a higher  $\alpha$ . This supports theory that trees growing in dense forests are competing for resources, reducing individual tree leaf area (Jump et al., 2017). The negative height –  $\alpha$  and positive CAI –  $\alpha$  relationships in our model suggest that trees may initially invest in vertical growth to reach the canopy level, and once there invest in lateral growth, with more leaf area, to increase light capture. This supports theory that trees grow to outcompete neighbouring individuals for light capture (Purves and Pacala, 2008) and evidence that both lateral growth and LAI are reduced beneath closed canopies (Beaudet and Messier, 1998; Canham, 1988).

Wood may be harder to accurately classify than leaves in TLS data (Vicari et al., 2019), resulting in a higher occurrence of false positives in wood clouds, potentially leading to an overestimation in WAI, and therefore underestimation of  $\alpha$ , especially in trees with small leaves which are prevalent in dry, Mediterranean environments (Peppe et al., 2011). The problem of misclassification will increase in taller trees due to TLS beam divergence, occlusion and larger beam footprint at further distances (Vicari et al., 2019), suggesting that WAI overestimation could be more pronounced in tall trees. Although our dense scanning strategy (Owen et al., 2021) was designed to mitigate some of these effects, it is possible our findings could underestimate the slope of the negative relationship between  $\alpha$  and tree height.

#### 4.6 Correcting for non-photosynthetic elements in LAI estimates using TLS

The value of TLS data to estimate individual tree PAI, WAI and subsequently  $\alpha$ , demonstrates their potential to corrective factors for non-photosynthetic components in ground based remote sensing measurements of LAI. Properly correcting for WAI in LAI estimates is of global importance as small errors in ground based measurements propagate through to large scale satellite observations generating large errors in global vegetation models (Calders et al., 2018). [The work presented here provides a foundation for future work combining multi-source and multi-scale remote sensing datasets to correct large-scale LAI products.](#) Our results echo others' in finding that the prevalence of woody material in the tree canopy, and therefore  $\alpha$ , is dynamic and varies by species as well as senescence, crown health and, in the case of deciduous forests, leaf phenology (Gower et al., 1999). The use of single  $\alpha$  value in a plot or region (Olivas et al., 2013; Woodgate et al., 2016), invariant of species, size and forest structure, to convert PAI to LAI is therefore problematic (Niu et al., 2021). Our study demonstrates the importance of taking species mix and structural variation into account when correcting for non-photosynthetic material in ground-based LAI estimates.

#### 5. Conclusions

We tested three methods for estimating PAI using Terrestrial Laser Scanning data and compared these against traditional DHP measurements. We found large variation between PAI values estimated from each TLS method and DHP, demonstrating that care should be taken when deriving PAI from ground based remote sensing methods. Although the *LiDAR Pulse* method was found to have the best agreement with both single scan and whole plot PAI values measured by DHP, the *Voxel-Based* method allowed separate analysis of the key metric used to correct for the effect of WAI in LAI measurements,  $\alpha$ , in individual trees. We recommend the *LiDAR Pulse* method as a fast and effective method for PAI estimation independent of illumination conditions. Whilst the *Voxel-Based* method may be used to analyse individual tree  $\alpha$  and determine ecological drivers of variation, work remains to

determine the validity of these approaches, in particular correct voxel size choice. We found that  $\alpha$  varies by species, height and stand density, showing the importance of accurately correcting for WAI on the individual tree level and the utility of TLS to do so.

The variation in our results for the different methods used to derive PAI from TLS data show that there is some way to go before TLS derived vegetation indices can be interpreted as robust and reliable. Validation using destructive samples and further intercomparison studies of methods are needed to demonstrate the advantages of TLS, and use of benchmarking datasets should be standard. DHP is a faster, cheaper and more widely accessible method for PAI estimation, and while TLS promises to alleviate potential bias in DHP estimates, results are highly methods dependent. Our results demonstrate the challenges that stand in the way of large scale adoption of TLS for vegetation indices monitoring.

## 6. Code availability

See [https://github.com/will-flynn/tls\\_dhp\\_pai.git](https://github.com/will-flynn/tls_dhp_pai.git) for all processing and modelling code.

## 7. Data availability

See Owen et al., (2022) for individual segmented tree data.

## 8. Author contribution

All authors designed the study. HJFO and WRMF collected and processed TLS and DHP data; WRMF performed formal analysis with guidance from all authors. WRMF led the writing with input from all authors. All authors contributed critically to drafts and gave final approval for publication.

## 9. Competing interests

The authors declare that they have no conflict of interest.

## 7. Acknowledgements

WRMF was funded through a London NERC DTP PhD studentship. ERL, HJFO and SWDG were funded through the UKRI Future Leaders Fellowship awarded to ERL (MR/T019832/1).

## References

- Baeten, L., Verheyen, K., Wirth, C., Bruelheide, H., Bussotti, F., Finér, L., Jaroszewicz, B., Selvi, F., Valladares, F., Allan, E., Ampoorter, E., Auge, H., Avăcăriei, D., Barbaro, L., Bărnoaiea, I., Bastias, C. C., Bauhus, J., Beinhoff, C., Benavides, R., Benneter, A., Berger, S., Berthold, F., Boberg, J., Bonal, D., Brüggemann, W., Carnol, M., Castagneyrol, B., Charbonnier, Y., Čečko, E., Coomes, D., Coppi, A., Dalmaris, E., Dănilă, G., Dawud, S. M., de Vries, W., De Wandeler, H., Deconchat, M., Domisch, T., Duduman, G., Fischer, M., Fotelli, M., Gessler, A., Gimeno, T. E., Granier, A., Grossiord, C., Guyot, V., Hantsch, L., Hättenschwiler, S., Hector, A., Hermy, M., Holland, V., Jactel, H., Joly, F.-X., Jucker, T., Kolb, S., Koricheva, J., Lexer, M. J., Liebergessell, M., Milligan, H., Müller, S., Muys, B., Nguyen, D., Nichiforel, L., Pollastrini, M., Proulx, R., Rabasa, S., Radoglou, K., Ratcliffe, S., Raulund-Rasmussen, K., Seiferling, I., Stenlid, J., Vesterdal, L., von Wilpert, K., Zavala, M. A., Zielinski, D., and Scherer-Lorenzen, M.: A novel comparative research platform designed to determine the functional significance of tree species diversity in European forests, *Persepect. Plant. Ecol.*, 15, 281–291, <https://doi.org/10.1016/j.ppees.2013.07.002>, 2013.
- Baret, F., Weiss, M., Lacaze, R., Camacho, F., Makhmara, H., Pacholczyk, P., and Smets, B.: GEOV1: LAI and FAPAR essential climate variables and FCOVER global time series capitalizing over existing products. Part1: Principles of development and production, *Remote Sens. Environ.*, 137, 299–309, <https://doi.org/10.1016/j.rse.2012.12.027>, 2013.



488 Bates, D., Mächler, M., Bolker, B., and Walker, S.: Fitting Linear Mixed-Effects Models Using lme4, *J. Stat.*  
489 *Softw.*, 67, <https://doi.org/10.18637/jss.v067.i01>, 2015.

490 Battaglia, M., Cherry, M. L., Beadle, C. L., Sands, P. J., and Hingston, A.: Prediction of leaf area index in  
491 eucalypt plantations: effects of water stress and temperature, *Tree Physiol.*, 18, 521–528,  
492 <https://doi.org/10.1093/treephys/18.8-9.521>, 1998.

493 Beaudet, M. and Messier, C.: Growth and morphological responses of yellow birch, sugar maple, and beech  
494 seedlings growing under a natural light gradient, *Can. J. Forest Res.*, 28, 1007–1015,  
495 <https://doi.org/10.1139/x98-077>, 1998.

496 Béland, M., Baldocchi, D. D., Widlowski, J.-L., Fournier, R. A., and Verstraete, M. M.: On seeing the wood  
497 from the leaves and the role of voxel size in determining leaf area distribution of forests with terrestrial LiDAR,  
498 *Agr. Forest Meteorol.*, 184, 82–97, <https://doi.org/10.1016/j.agrformet.2013.09.005>, 2014.

499 Breda, N. J. J.: Ground-based measurements of leaf area index: a review of methods, instruments and current  
500 controversies, *J. Exp. Bot.*, 54, 2403–2417, <https://doi.org/10.1093/jxb/erg263>, 2003.

501 Burt, A., Disney, M., and Calders, K.: Extracting individual trees from lidar point clouds using treeseg, *Methods*  
502 *Ecol. Evol.*, 10, 438–445, <https://doi.org/10.1111/2041-210X.13121>, 2019.

503 Calders, K., Armston, J., Newnham, G., Herold, M., and Goodwin, N.: Implications of sensor configuration and  
504 topography on vertical plant profiles derived from terrestrial LiDAR, *Agr. Forest Meteorol.*, 194, 104–117,  
505 <https://doi.org/10.1016/j.agrformet.2014.03.022>, 2014.

506 Calders, K., Origo, N., Disney, M., Nightingale, J., Woodgate, W., Armston, J., and Lewis, P.: Variability and  
507 bias in active and passive ground-based measurements of effective plant, wood and leaf area index, *Agr. Forest*  
508 *Meteorol.*, 252, 231–240, <https://doi.org/10.1016/j.agrformet.2018.01.029>, 2018.

509 Calders, K., Adams, J., Armston, J., Bartholomeus, H., Bauwens, S., Bentley, L. P., Chave, J., Danson, F. M.,  
510 Demol, M., Disney, M., Gaulton, R., Krishna Moorthy, S. M., Levick, S. R., Saarinen, N., Schaaf, C., Stovall,  
511 A., Terryn, L., Wilkes, P., and Verbeeck, H.: Terrestrial laser scanning in forest ecology: Expanding the  
512 horizon, *Remote Sensing of Environment*, 251, 112102, <https://doi.org/10.1016/j.rse.2020.112102>, 2020.

513 Canham, C. D.: Growth and Canopy Architecture of Shade-Tolerant Trees: Response to Canopy Gaps, *Ecology*,  
514 69, 786–795, <https://doi.org/10.2307/1941027>, 1988.

515 Carter, J. L. and White, D. A.: Plasticity in the Huber value contributes to homeostasis in leaf water relations of  
516 a mallee Eucalypt with variation to groundwater depth, *Tree Physiol.*, 29, 1407–1418,  
517 <https://doi.org/10.1093/treephys/tpp076>, 2009.

518 Caspersen, J. P., Vanderwel, M. C., Cole, W. G., and Purves, D. W.: How Stand Productivity Results from Size-  
519 and Competition-Dependent Growth and Mortality, *PLoS ONE*, 6, e28660,  
520 <https://doi.org/10.1371/journal.pone.0028660>, 2011.

521 Castro-Díez, P., Villar-Salvador, P., Pérez-Rontomé, C., Maestro-Martínez, M., and Montserrat-Martí, G.: Leaf  
522 morphology and leaf chemical composition in three *Quercus* (Fagaceae) species along a rainfall gradient in NE  
523 Spain, *Trees*, 11, 127–134, <https://doi.org/10.1007/PL00009662>, 1997.

524 Chen, J. M. and Black, T. A.: Defining leaf area index for non-flat leaves, *Plant Cell Environ.*, 15, 421–429,  
525 <https://doi.org/10.1111/j.1365-3040.1992.tb00992.x>, 1992.

526 Coomes, D. A., Holdaway, R. J., Kobe, R. K., Lines, E. R., and Allen, R. B.: A general integrative framework  
527 for modelling woody biomass production and carbon sequestration rates in forests, *Journal of Ecology*, 100, 42–  
528 64, <https://doi.org/10.1111/j.1365-2745.2011.01920.x>, 2012.

529 Disney, M.: Terrestrial LiDAR: a three-dimensional revolution in how we look at trees, *New Phytol.*, 222,  
530 1736–1741, <https://doi.org/10.1111/nph.15517>, 2018.

531 Gazal, R. M., Scott, R. L., Goodrich, D. C., and Williams, D. G.: Controls on transpiration in a semiarid riparian  
532 cottonwood forest, *Agr. Forest Meterol.*, 137, 56–67, <https://doi.org/10.1016/j.agrformet.2006.03.002>, 2006.

533 Gower, S. T., Vogel, J. G., Norman, J. M., Kucharik, C. J., Steele, S. J., and Stow, T. K.: Carbon distribution  
534 and aboveground net primary production in aspen, jack pine, and black spruce stands in Saskatchewan and  
535 Manitoba, Canada, *J. Geophys. Res.*, 102, 29029–29041, <https://doi.org/10.1029/97JD02317>, 1997.

536 Gower, S. T., Kucharik, C. J., and Norman, J. M.: Direct and Indirect Estimation of Leaf Area Index, fAPAR,  
537 and Net Primary Production of Terrestrial Ecosystems, *Remote Sens. Environ.*, 70, 29–51,  
538 [https://doi.org/10.1016/S0034-4257\(99\)00056-5](https://doi.org/10.1016/S0034-4257(99)00056-5), 1999.

539 Grotti, M., Calders, K., Origo, N., Puletti, N., Alivernini, A., Ferrara, C., and Chianucci, F.: An intensity, image-  
540 based method to estimate gap fraction, canopy openness and effective leaf area index from phase-shift terrestrial  
541 laser scanning, *Agr. Forest Meterol.*, 280, 107766, <https://doi.org/10.1016/j.agrformet.2019.107766>, 2020.

542 Hardwick, S. R., Toumi, R., Pfeifer, M., Turner, E. C., Nilus, R., and Ewers, R. M.: The relationship between  
543 leaf area index and microclimate in tropical forest and oil palm plantation: Forest disturbance drives changes in  
544 microclimate, *Agr. Forest Meterol.*, 201, 187–195, <https://doi.org/10.1016/j.agrformet.2014.11.010>, 2015.

545 Hijmans, R. J.: raster: Geographic Data Analysis and Modeling R package version 3.5-21, [https://CRAN.R-](https://CRAN.R-project.org/package=raster)  
546 [project.org/package=raster](https://CRAN.R-project.org/package=raster), 2022.

547 Hosoi, F. and Omasa, K.: Voxel-Based 3-D Modeling of Individual Trees for Estimating Leaf Area Density  
548 Using High-Resolution Portable Scanning Lidar, *IEEE T. Geosci. Remote*, 44, 3610–3618,  
549 <https://doi.org/10.1109/TGRS.2006.881743>, 2006.

550 Itakura, K. and Hosoi, F.: Voxel-based leaf area estimation from three-dimensional plant images, *J. Agric.*  
551 *Meteorol.*, 75, 211–216, <https://doi.org/10.2480/agrmet.d-19-00013>, 2019.

552 Jonckheere, I., Fleck, S., Nackaerts, K., Muys, B., Coppin, P., Weiss, M., and Baret, F.: Review of methods for  
553 in situ leaf area index determination, *Agr. Forest Meterol.*, 121, 19–35,  
554 <https://doi.org/10.1016/j.agrformet.2003.08.027>, 2004.

555 Jonckheere, I. G. C., Muys, B., and Coppin, P.: Allometry and evaluation of in situ optical LAI determination in  
556 Scots pine: a case study in Belgium, *Tree Physiol.*, 25, 723–732, <https://doi.org/10.1093/treephys/25.6.723>,  
557 2005.

558 Jucker, T., Bouriaud, O., Avacaritei, D., Dănilă, I., Duduman, G., Valladares, F., and Coomes, D. A.:  
559 Competition for light and water play contrasting roles in driving diversity-productivity relationships in Iberian  
560 forests, *J. Ecol.*, 102, 1202–1213, <https://doi.org/10.1111/1365-2745.12276>, 2014.

561 Jump, A. S., Ruiz-Benito, P., Greenwood, S., Allen, C. D., Kitzberger, T., Fensham, R., Martínez-Vilalta, J.,  
562 and Lloret, F.: Structural overshoot of tree growth with climate variability and the global spectrum of drought-  
563 induced forest dieback, *Glob. Change Biol.*, 23, 3742–3757, <https://doi.org/10.1111/gcb.13636>, 2017.

564 Jupp, D. L. B., Culvenor, D. S., Lovell, J. L., Newnham, G. J., Strahler, A. H., and Woodcock, C. E.: Estimating  
565 forest LAI profiles and structural parameters using a ground-based laser called 'Echidna(R)', *Tree Physiol.*, 29,  
566 171–181, <https://doi.org/10.1093/treephys/tpn022>, 2008.

567 Kamoske, A. G., Dahlin, K. M., Stark, S. C., and Serbin, S. P.: Leaf area density from airborne LiDAR:  
568 Comparing sensors and resolutions in a temperate broadleaf forest ecosystem, *Forest Ecol. Manag.*, 433, 364–  
569 375, <https://doi.org/10.1016/j.foreco.2018.11.017>, 2019.

570 Kuusk, V., Niinemets, Ü., and Valladares, F.: A major trade-off between structural and photosynthetic  
571 investments operative across plant and needle ages in three Mediterranean pines, *Tree Physiol.*, 38, 543–557,  
572 <https://doi.org/10.1093/treephys/tpx139>, 2018.

573 Leblanc, S. G. and Chen, J. M.: A practical scheme for correcting multiple scattering effects on optical LAI  
574 measurements, *Agr. Forest Meterol.*, 110, 125–139, [https://doi.org/10.1016/S0168-1923\(01\)00284-2](https://doi.org/10.1016/S0168-1923(01)00284-2), 2001.

575 Lecigne, B., Delagrangé, S., and Messier, C.: Exploring trees in three dimensions: VoxR, a novel voxel-based R  
576 package dedicated to analysing the complex arrangement of tree crowns, *Ann. Bot-London*, 121, 589–601,  
577 <https://doi.org/10.1093/aob/mcx095>, 2018.

578 Li, S., Dai, L., Wang, H., Wang, Y., He, Z., and Lin, S.: Estimating Leaf Area Density of Individual Trees  
579 Using the Point Cloud Segmentation of Terrestrial LiDAR Data and a Voxel-Based Model, *Remote Sens-Basel*,  
580 9, 1202, <https://doi.org/10.3390/rs9111202>, 2017.

581 Li, Y., Guo, Q., Tao, S., Zheng, G., Zhao, K., Xue, B., and Su, Y.: Derivation, Validation, and Sensitivity  
582 Analysis of Terrestrial Laser Scanning-Based Leaf Area Index, *Can. J. Remote Sens.*, 42, 719–729,  
583 <https://doi.org/10.1080/07038992.2016.1220829>, 2016.

584 Lines, E. R., Fischer, F. J., Owen, H. J. F., and Jucker, T.: The shape of trees: Reimagining forest ecology in  
585 three dimensions with remote sensing, *J. Ecol.*, 110, 1730–1745, <https://doi.org/10.1111/1365-2745.13944>,  
586 2022.

587 Long, J. N. and Smith, F. W.: Leaf area - sapwood area relations of lodgepole pine as influenced by stand  
588 density and site index., *Can. J. Forest Res.*, 18, 247–250, 1988.

589 López, R., Cano, F. J., Martin-StPaul, N. K., Cochard, H., and Choat, B.: Coordination of stem and leaf traits  
590 define different strategies to regulate water loss and tolerance ranges to aridity, *New Phytol.*, 230, 497–509,  
591 <https://doi.org/10.1111/nph.17185>, 2021.

592 Lovell, J. L., Jupp, D. L. B., van Gorsel, E., Jimenez-Berni, J., Hopkinson, C., and Chasmer, L.: Foliage Profiles  
593 from Ground Based Waveform and Discrete Point Lidar, *SilviLaser*, 1–9, 2011.

594 Ma, L., Zheng, G., Eitel, J. U. H., Magney, T. S., and Moskal, L. M.: Determining woody-to-total area ratio  
595 using terrestrial laser scanning (TLS), *Agr. Forest Meteorol.*, 228–229, 217–228,  
596 <https://doi.org/10.1016/j.agrformet.2016.06.021>, 2016.

597 Madrigal-González, J., Herrero, A., Ruiz-Benito, P., and Zavala, M. A.: Resilience to drought in a dry forest:  
598 Insights from demographic rates, *Forest Ecol. Manag.*, 389, 167–175,  
599 <https://doi.org/10.1016/j.foreco.2016.12.012>, 2017.

600 Magnani, F., Mencuccini, M., and Grace, J.: Age-related decline in stand productivity: the role of structural  
601 acclimation under hydraulic constraints, *Plant Cell Environ.*, 23, 251–263, <https://doi.org/10.1046/j.1365-3040.2000.00537.x>, 2000.

603 Mencuccini, M.: The ecological significance of long-distance water transport: short-term regulation, long-term  
604 acclimation and the hydraulic costs of stature across plant life forms, *Plant Cell Environ.*, 26, 163–182,  
605 <https://doi.org/10.1046/j.1365-3040.2003.00991.x>, 2003.

606 Mencuccini, M. and Grace, J.: Climate influences the leaf area/sapwood area ratio in Scots pine, *Tree Physiol.*,  
607 15, 1–10, <https://doi.org/10.1093/treephys/15.1.1>, 1995.

608 Monsi, M. and Saeki, T.: On the Factor Light in Plant Communities and its Importance for Matter Production,  
609 *Ann. Bot-London*, 95, 549–567, <https://doi.org/10.1093/aob/mci052>, 1953.

610 Nakagawa, S., Johnson, P. C. D., and Schielzeth, H.: The coefficient of determination R<sup>2</sup> and intra-class  
611 correlation coefficient from generalized linear mixed-effects models revisited and expanded, *J. R. Soc.  
612 Interface*, 14, 20170213, <https://doi.org/10.1098/rsif.2017.0213>, 2017.

613 Niinemets, Ü. and Valladares, F.: Tolerance to shade, drought, and waterlogging of temperate northern  
614 hemisphere trees and shrubs, *Ecol. Monogr.*, 76, 521–547, [https://doi.org/10.1890/0012-9615\(2006\)076\[0521:TTSDAW\]2.0.CO;2](https://doi.org/10.1890/0012-9615(2006)076[0521:TTSDAW]2.0.CO;2), 2006.

616 Niu, X., Fan, J., Luo, R., Fu, W., Yuan, H., and Du, M.: Continuous estimation of leaf area index and the  
617 woody-to-total area ratio of two deciduous shrub canopies using fisheye webcams in a semiarid loessial region  
618 of China, *Ecol. Indic.*, 125, 107549, <https://doi.org/10.1016/j.ecolind.2021.107549>, 2021.

619 Olivas, P. C., Oberbauer, S. F., Clark, D. B., Clark, D. A., Ryan, M. G., O'Brien, J. J., and Ordoñez, H.:  
620 Comparison of direct and indirect methods for assessing leaf area index across a tropical rain forest landscape,  
621 *Agr. Forest Meteorol.*, 177, 110–116, <https://doi.org/10.1016/j.agrformet.2013.04.010>, 2013.

622 Owen, H. J. F., Flynn, W. R. M., and Lines, E. R.: Competitive drivers of inter-specific deviations of crown  
623 morphology from theoretical predictions measured with Terrestrial Laser Scanning, *J. Ecol.*, 109, 2612–2628,  
624 <https://doi.org/10.1111/1365-2745.13670>, 2021.

625 Owen, H. J. F., Flynn, W. R. M., and Lines, E. R.: Individual TLS tree clouds collected from both Alto Tajo and  
626 Cuellar in Spain., [10.5281/zenodo.6962717](https://doi.org/10.5281/zenodo.6962717), 2022.

627 Peppe, D. J., Royer, D. L., Cariglino, B., Oliver, S. Y., Newman, S., Leight, E., Enikolopov, G., Fernandez-  
628 Burgos, M., Herrera, F., Adams, J. M., Correa, E., Currano, E. D., Erickson, J. M., Hinojosa, L. F., Hoganson, J.  
629 W., Iglesias, A., Jaramillo, C. A., Johnson, K. R., Jordan, G. J., Kraft, N. J. B., Lovelock, E. C., Lusk, C. H.,  
630 Niinemets, Ü., Peñuelas, J., Rapson, G., Wing, S. L., and Wright, I. J.: Sensitivity of leaf size and shape to  
631 climate: global patterns and paleoclimatic applications, *New Phytol.*, 190, 724–739,  
632 <https://doi.org/10.1111/j.1469-8137.2010.03615.x>, 2011.

633 Pfeifer, M., Gonsamo, A., Disney, M., Pellikka, P., and Marchant, R.: Leaf area index for biomes of the Eastern  
634 Arc Mountains: Landsat and SPOT observations along precipitation and altitude gradients, *Remote Sens.*  
635 *Environ.*, 118, 103–115, <https://doi.org/10.1016/j.rse.2011.11.009>, 2012.

636 Phillips, N., Bond, B. J., McDowell, N. G., Ryan, M. G., and Schauer, A.: Leaf area compounds height-related  
637 hydraulic costs of water transport in Oregon White Oak trees, *Funct. Ecol.*, 17, 832–840,  
638 <https://doi.org/10.1111/j.1365-2435.2003.00791.x>, 2003.

639 Purves, D. and Pacala, S.: Predictive Models of Forest Dynamics, *Science*, 320, 1452–1453,  
640 <https://doi.org/10.1126/science.1155359>, 2008.

641 Ridler, T. W. and Calvard, S.: Picture Thresholding Using an Iterative Selection Method, *IEEE T. Syst. Man.*  
642 *Cyb.*, 8, 630–632, <https://doi.org/10.1109/TSMC.1978.4310039>, 1978.

643 Sea, W. B., Choler, P., Beringer, J., Weinmann, R. A., Hutley, L. B., and Leuning, R.: Documenting  
644 improvement in leaf area index estimates from MODIS using hemispherical photos for Australian savannas,  
645 *Agr. Forest Meteorol.*, 151, 1453–1461, <https://doi.org/10.1016/j.agrformet.2010.12.006>, 2011.

646 Specht, R. L. and Specht, A.: Canopy structure in Eucalyptus-dominated communities in Australia along  
647 climatic gradients, Canopy structure in Eucalyptus-dominated communities in Australia along climatic  
648 gradients, 10, 191–213, 1989.

649 Vicari, M. B., Disney, M., Wilkes, P., Burt, A., Calders, K., and Woodgate, W.: Leaf and wood classification  
650 framework for terrestrial LiDAR point clouds, *Methods Ecol. Evol.*, 10, 680–694, <https://doi.org/10.1111/2041-210X.13144>, 2019.

652 Warton, D. I., Wright, I. J., Falster, D. S., and Westoby, M.: Bivariate line-fitting methods for allometry, *Biol.*  
653 *Rev.*, 81, 259–291, <https://doi.org/10.1017/S1464793106007007>, 2006.

654 Warton, D. I., Duursma, R. A., Falster, D. S., and Taskinen, S.: smatr 3 - an R package for estimation and  
655 inference about allometric lines: *The smatr 3 - an R package*, *Methods Ecol. Evol.*, 3, 257–259,  
656 <https://doi.org/10.1111/j.2041-210X.2011.00153.x>, 2012.

657 Weiss, M., Baret, F., Smith, G. J., Jonckheere, I., and Coppin, P.: Review of methods for in situ leaf area index  
658 (LAI) determination, *Agr. Forest Meteorol.*, 121, 37–53, <https://doi.org/10.1016/j.agrformet.2003.08.001>, 2004.

659 Whitehead, D.: The Estimation of Foliage Area from Sapwood Basal Area in Scots Pine, *Forestry*, 51, 137–149,  
660 <https://doi.org/10.1093/forestry/51.2.137>, 1978.

661 Wilkes, P., Lau, A., Disney, M., Calders, K., Burt, A., Gonzalez de Tanago, J., Bartholomeus, H., Brede, B., and  
662 Herold, M.: Data acquisition considerations for Terrestrial Laser Scanning of forest plots, *Remote Sensing of*  
663 *Environment*, 196, 140–153, <https://doi.org/10.1016/j.rse.2017.04.030>, 2017.

664 Woodgate, W., Jones, S. D., Suarez, L., Hill, M. J., Armston, J. D., Wilkes, P., Soto-Berelev, M., Haywood, A.,  
 665 and Mellor, A.: Understanding the variability in ground-based methods for retrieving canopy openness, gap  
 666 fraction, and leaf area index in diverse forest systems, *Agr. Forest Meterol.*, 205, 83–95,  
 667 <https://doi.org/10.1016/j.agrformet.2015.02.012>, 2015.

668 Woodgate, W., Armston, J. D., Disney, M., Jones, S. D., Suarez, L., Hill, M. J., Wilkes, P., and Soto-Berelev,  
 669 M.: Quantifying the impact of woody material on leaf area index estimation from hemispherical photography  
 670 using 3D canopy simulations, *Agr. Forest Meterol.*, 226–227, 1–12,  
 671 <https://doi.org/10.1016/j.agrformet.2016.05.009>, 2016.

672 Zhang, Y., Chen, J. M., and Miller, J. R.: Determining digital hemispherical photograph exposure for leaf area  
 673 index estimation, *Agr. Forest Meterol.*, 133, 166–181, <https://doi.org/10.1016/j.agrformet.2005.09.009>, 2005.

674 Zheng, G., Moskal, L. M., and Kim, S.-H.: Retrieval of Effective Leaf Area Index in Heterogeneous Forests  
 675 With Terrestrial Laser Scanning, *IEEE T. Geosci. Remote*, 51, 777–786,  
 676 <https://doi.org/10.1109/TGRS.2012.2205003>, 2013.

677 Zhu, X., Skidmore, A. K., Wang, T., Liu, J., Darvishzadeh, R., Shi, Y., Premier, J., and Heurich, M.: Improving  
 678 leaf area index (LAI) estimation by correcting for clumping and woody effects using terrestrial laser scanning,  
 679 *Agr. Forest Meterol.*, 263, 276–286, <https://doi.org/10.1016/j.agrformet.2018.08.026>, 2018.

680

## Appendix A

Table 1: species –  $\alpha$  linear mixed model (equation 1) showing relationship between tree species and  $\alpha$  for all 2472 individual trees. Species are listed from low – high drought tolerance, with the exception of *P. pinaster*, for which drought tolerance index has not been calculated in the literature.

Species	$\alpha$ (eq. 1)	95% CI
<i>P. sylvestris</i>	0.144	0.131, 0.158
<i>P. nigra</i>	0.138	0.127, 0.149
<i>Q. faginea</i>	0.149	0.140, 0.157
<i>Q. ilex</i>	0.155	0.146, 0.166
<i>P. pinaster</i>	0.168	0.145, 0.192

Table 2: height –  $\alpha$  linear mixed models for each species (equation 2) showing relationship between tree height and plot CAI and  $\alpha$  for all 2472 individual trees. Species are listed from low – high estimated  $\alpha$ . Significance codes:  $p < 0.001$  ‘\*\*\*’;  $p < 0.01$  ‘\*\*’;  $p < 0.05$  ‘\*’; not significant ‘ns’

Species	$b$ (eq. 2) (95% CI)	$c$ (eq. 2) (95% CI)	ICC
<i>P. sylvestris</i>	-0.002 <sup>ns</sup> (-0.004, 0.000)	0.134 <sup>ns</sup> (0.010, 0.259)	0.151
<i>P. nigra</i>	-0.005*** (-0.006, -0.004)	0.164** (0.063, 0.263)	0.211
<i>Q. faginea</i>	-0.008*** (-0.010, -0.007)	0.058* (0.016, 0.101)	0.060
<i>Q. ilex</i>	-0.015*** (-0.020, -0.011)	0.113** (0.050, 0.179)	0.070
<i>P. pinaster</i>	-0.006*** (-0.008, -0.004)	0.317* (0.177, 0.453)	0.036

## Appendix B

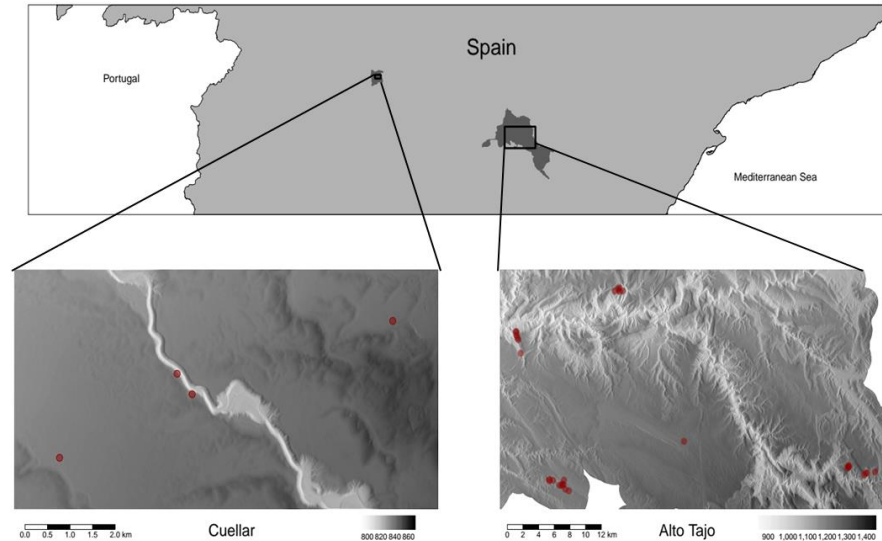


Figure 1: Map of plot locations within two field sites in central Spain (Cuellar, left and Alto Tajo, right). Red points show plot locations on high-resolution digital terrain models enhanced with hillshading shown in greyscale.

## Appendix C

$$WAI = m_{species} + b \quad (1)$$

$$WAI = m_{height} + b \quad (2)$$

$$WAI = m_{CAI} + b \quad (3)$$

$$WAI = m_{PAI} + b \quad (4)$$

Where WAI is the wood area index, *species*, *height*, *CAI* and *PAI* are the tree species, tree height, crown area index of the plot in which the tree is growing and tree plant area index respectively and *m* and *b* are parameters to be fit.

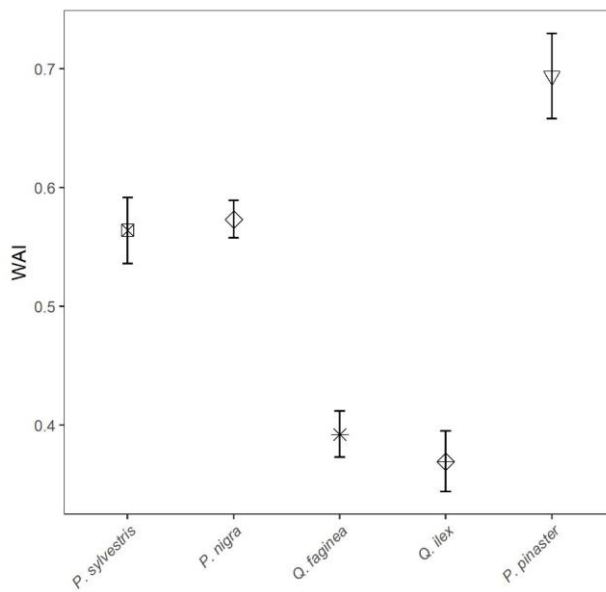


Figure 2: Linear model derived WAI values (*m*, equation C1) for all 2472 individual trees of species *P. sylvestris*, *P. nigra*, *Q. faginea*, *Q. ilex* and *P. pinaster*. Error bars represent 95% confidence intervals. Species are listed from low – high drought tolerance, with the exception of *P. pinaster*, for which drought tolerance index has not been calculated in the literature.

Table 3: Linear model (equation C1) showing relationship between tree species and WAI for all 2471 individual trees. Significance codes:  $p < 0.001$  '\*\*\*';  $p < 0.01$  '\*\*';  $p < 0.05$  '\*'; not significant 'ns'

Species	<i>m</i> (eq. 1)	Std. Error	P value
<i>P.nigra</i>	0.57	0.008	***
<i>P. pinaster</i>	0.69	0.018	
<i>P. sylvestris</i>	0.56	0.014	
<i>Q. faginea</i>	0.39	0.010	***
<i>Q. ilex</i>	0.37	0.013	***

**Table 4: Linear models (equations C2, C3, C4) predicting WAI as a function of tree height, CAI (density) and PAI**  
Significance codes:  $p < 0.001$  ‘\*\*\*’;  $p < 0.01$  ‘\*\*’;  $p < 0.05$  ‘\*’; not significant ‘ns’

	$m$ (eq. 2, 3, 4)	$R^2$	P value
Tree Height	0.02	0.27	***
CAI	0.39	0.78	***
PAI	0.11	0.35	***